Uptake of exogenous serine is important to maintain sphingolipid homeostasis in *Saccharomyces cerevisiae*

Bianca M. Esch[1], Sergej Limar[1], André Bogdanowski[2,3], Christos Gournas[4,#a], Tushar More[5], Celine Sundag[1], Stefan Walter[6], Jürgen J. Heinisch[7], Christer S. Ejsing[5,8], Bruno André[4] and Florian Fröhlich[1,6*]

[1]Department of Biology/Chemistry, Molecular Membrane Biology Group, University of Osnabrück, Barbarastraße 13, 49076 Osnabrück, Germany

[2]Department of Biology/Chemistry, Ecology Group, University of Osnabrück, Barbarastraße 13, 49076 Osnabrück, Germany

[3]UFZ–Helmholtz Centre for Environmental Research Ltd, Department for Ecological Modelling, Permoserstr. 15, 04318, Leipzig, Germany

[4]Molecular Physiology of the Cell, Université Libre de Bruxelles (ULB), Institut de Biologie et de Médecine Moléculaires, 6041 Gosselies, Belgium

[5]Department of Biochemistry and Molecular Biology, Villum Center for Bioanalytical Sciences, University of Southern Denmark, 5000 Odense, Denmark

[6]Center of Cellular Nanoanalytics Osnabrück, Barbarastraße 11, 49076 Osnabrück, Germany

[7]Department of Biology/Chemistry, Division of Genetics, University of Osnabrück, Barbarastraße 11, 49076 Osnabrück, Germany

[8]Cell Biology and Biophysics Unit, European Molecular Biology Laboratory, 69117 Heidelberg, Germany

[*]Corresponding author:

Email: florian.froehlich@biologie.uni-osnabrueck.de

Phone: +49-541-969-2961

[#a]Current address:
Microbial Molecular Genetics Laboratory
Institute of Biosciences and Applications (IBA)
National Centre for Scientific Research “Demokritos” (NCSRD)
Patr. Grigoriou E & 27 Neapoleos St., 15341 Agia Paraskevi, Greece

Abstract

Sphingolipids are abundant and essential molecules in eukaryotes that have crucial functions as signaling molecules and as membrane components. Sphingolipid biosynthesis starts in the endoplasmic reticulum with the condensation of serine and palmitoyl-CoA. Sphingolipid biosynthesis is highly regulated to maintain sphingolipid homeostasis. Even though, serine is an essential component of the sphingolipid biosynthesis pathway, its role in maintaining sphingolipid homeostasis has not been precisely studied. Here we show that serine uptake is an important factor for the regulation of sphingolipid biosynthesis in *Saccharomyces cerevisiae*. Using genetic experiments, we find the broad-specificity amino acid permease Gnp1 to be important for serine uptake. We confirm these results with serine uptake assays in *gnp1Δ* cells. We further show that uptake of exogenous serine by Gnp1 is important to maintain cellular serine levels and observe a specific connection between serine uptake and the first step of sphingolipid biosynthesis. Using mass spectrometry-based flux analysis, we further observed imported serine as the main source for *de novo* sphingolipid biosynthesis. Our results demonstrate that yeast cells preferentially use the uptake of exogenous serine to regulate sphingolipid biosynthesis. Our study can also be a starting point to analyze the role of serine uptake in mammalian sphingolipid metabolism.

Author Summary

Sphingolipids (SPs) are membrane lipids globally required for eukaryotic life. In contrast to other lipid classes, SPs cannot be stored in the cell and therefore their levels have to be tightly regulated. Failure to maintain sphingolipid homeostasis can result in pathologies including neurodegeneration, childhood asthma and cancer. However, we are only starting to understand how SP biosynthesis is adjusted according to need. In this study, we use genetic and biochemical methods to show that the uptake of exogenous serine is necessary to maintain SP homeostasis in *Saccharomyces cerevisiae*. Serine is one of the precursors of long chain bases in cells, the first intermediate of SP metabolism. Our results suggest that the uptake of serine is directly coupled to SP biosynthesis at ER-plasma membrane contact sites. Overall, our study identifies serine uptake as a novel regulatory factor of SP homeostasis. While we use yeast as a discovery tool, these results also provide valuable insights into mammalian SP biology especially under pathological conditions.

Introduction

Sphingolipids (SPs) are essential structural components of membranes and can also act as signaling molecules. SPs constitute up to 20% of the plasma membrane lipids and form tightly packed lipid bilayers together with sterols in the outer layer of the plasma membrane [1]. In contrast to glycerol-phospholipids (GPLs) and sterols, SPs cannot be stored in the cell. Thus, maintaining SP homeostasis is crucial to sustain membrane integrity and trafficking.

SPs are synthesized at the ER by two metabolic branches in yeast. In one branch, the serine palmitoyltransferase (SPT) catalyzes the condensation of serine and palmitoyl-CoA to yield 3-ketodihydrosphingosine. This short-lived intermediate is directly processed to long chain bases (LCBs). In a second branch, palmitoyl-CoA is elongated to up to 24 or 26 carbons chain length, the very long chain fatty acids (VLCFAs). LCBs and VLCFAs are amide linked to form ceramide [2]. In mammalian cells, ceramide transfer protein (CERT) transports ceramides to the Golgi apparatus [3]. A similar mechanism may occur in yeast cells, but the corresponding ceramide transfer protein has yet to be identified. Nvj2 has been suggested as a possible candidate transfer protein in this context [4]. At the yeast Golgi apparatus, ceramides receive various head groups to yield complex SPs. Complex SPs are transported from the Golgi apparatus to reach their destination at the plasma membrane by vesicular transport [5].

SP levels are regulated by post-translational modifications of key enzymes involved in their synthesis. When SP levels at the plasma membrane are low, the target of rapamycin complex 2 (TORC2) is activated and phosphorylates the yeast Akt homologue Ypk1 (reviewed in Heinisch and Rodicio, 2018). This leads to phosphorylation of the Orm proteins, negative regulators of the SPT, and releases the inhibition of SP biosynthesis [7–9]. Other mechanisms include the regulation of ceramide biosynthesis by Ypk kinases [10], the regulation of Pkh kinases [11], and the regulation of VLCFA biosynthesis [12,13]. Phospho-proteomic studies of SP homeostasis further suggested that the complex SP biosynthetic enzymes are also subject to regulation [14].

In fact, SP metabolism in yeast is regulated at several steps. However, little is known about the role of serine, one of the two substrates of the first and rate-limiting step in this pathway. Serine can be synthesized via the 3-phospho-glycerate pathway [15] or converted from glycine in a reversible reaction catalyzed by the serine hydroxymethyltransferases Shm1 and Shm2 [16]. Additionally, serine can be imported from the medium by plasma membrane permeases, as suggested by overexpression of the encoding genes [17]. Which portion of the different serine pools are incorporated into SPs is unknown. However, serine uptake and flux into the SP biosynthesis pathway has been shown to increase upon heat stress [18]. Interestingly, the catabolic serine deaminase Cha1 is upregulated by exogenous serine, and LCBs may serve as sensors of serine availability and mediate up-regulation of Cha1 in this response [19]. This indicates a regulatory control between exogenous serine and SP metabolism.

We therefore investigated the role of serine as an additional regulatory factor for SP homeostasis. We analyzed the impact of Gnp1 and Agp1, members of the yeast amino acid transporter (YAT) family [20], on serine uptake and intracellular amino acid concentrations and studied their role in SP homeostasis. Both proteins are dispensable for SP homeostasis under standard growth conditions. However, when SP metabolism is challenged by inhibition of the first steps in the synthetic pathway, Gnp1-dependent serine uptake becomes essential. Using mass spectrometry-based flux analysis we demonstrated the direct integration of imported serine into SPs and found extracellular serine to be the main source for *de novo* SP biosynthesis. Combined, these data reveal an additional, previously unknown, regulatory mechanism to maintain cellular SP homeostasis.

Results

Serine is required for SP homeostasis

SP biosynthesis starts with the condensation of serine and palmitoyl-CoA by the rate limiting enzyme SPT. Serine can be synthesized from 3-phospho-glycerate via reactions

145 catalyzed by Ser3/Ser33, Ser1 and Ser2 (Fig 1a) or from glycine by the action of the serine
146 hydroxymethyltransferases Shm1 and Shm2 [16]. To assess the effects of altered serine
147 availability we first tested whether deletion mutants of the 3-phospho-glycerate pathway are
148 auxotroph for serine under different conditions. For this purpose, all available serine
149 biosynthesis mutants from the yeast deletion collection [21] were spotted onto the respective
150 drop-out media. When *SER1* or *SER2* were deleted, cells did not grow on medium lacking
151 serine, while single mutants in the redundant gene pair (*ser3Δ* or *ser33Δ*) were able to grow
152 (Fig 1b). This confirms the previously observed serine auxotrophy for a single *SER1* or *SER2*
153 deletion [22].

154 In a genome wide chemical genetic screen we had previously identified a *ser2Δ* strain
155 as sensitive to the depletion of SPs by myriocin [23]. Myriocin is a suicide inhibitor of the SPT,
156 consisting of the subunits Lcb1, Lcb2 and the regulatory subunit Tsc3 (Fig 1c, [24] . We
157 therefore tested growth of a *ser2Δ* strain and a wild-type (WT) strain on control plates, plates
158 lacking serine, plates containing myriocin and plates containing myriocin and lacking serine.
159 As shown in Fig 1d, *ser2Δ* cells were highly sensitive to chemical depletion of SPs by myriocin,
160 demonstrating the importance of serine availability for the maintenance of SP homeostasis. In
161 addition, media without serine renders WT cells more sensitive to chemical depletion of SPs
162 (Fig 1d), suggesting that the presence of exogenous serine is also an important factor to
163 maintain SP homeostasis.

164 ## *GNP1* genetically interacts with serine metabolic genes in yeast

165 Due to the essential nature of serine for metabolism, one would expect that a defect in a major
166 serine permease would be lethal for a serine auxotroph strain. In contrast, impairment of either
167 serine uptake or serine biosynthesis should be tolerable under growth conditions where serine
168 is available (Fig 2a). We therefore specifically screened high throughput genetic interaction
169 data for interactions with a *ser2Δ* deletion [25]. We plotted the genetic interaction score of
170 *ser2Δ* (epsilon score) with each gene deletion against the significance of the genetic interaction
171 (Fig 2b; note that similar results were obtained for *ser1Δ*). Interestingly, the strongest and most

significant genetic interaction of the *SER2* gene was observed with two ORFs, *GNP1* and *YDR509W*, with the latter being annotated as a dubious open reading frame partially overlapping with *GNP1*.

Other significant hits were part of the TORC1 signaling pathway (S1 Fig). In line with our hypothesis, *GNP1* encodes a broad-specificity amino acid permease that was previously suggested to be necessary for the uptake of serine and other amino acids [17].

We proceeded by studying the genetic interaction of *SER2* and *GNP1* using tetrad analyses. As expected, the double knockout of *ser2Δgnp1Δ* showed a very strong negative genetic interaction as reflected by slow growth and very small colonies (Fig 2c). *GNP1* has a paralog, *AGP1,* which was presumably generated by the whole genome duplication in *S. cerevisiae* [26]. The respective epistasis analysis with the *ser2Δ* mutant did not reveal any synthetic phenotype (Fig 2d), suggesting that Gnp1 is the major permease with regard to serine uptake. The fact that the triple knockout *ser2Δgnp1Δagp1Δ* mutants did not produce any viable progeny indicates a complete lack of serine import in the absence of both permeases, Agp1 and Gnp1 (Fig 2e).

Gnp1 is the major serine transporters in yeast cells

Our genetic analyses suggested Gnp1 to be the major serine permease in yeast with only minor contributions of its paralog Agp1. This was confirmed by determination of serine uptake kinetics with radioactively labelled serine in *gnp1Δ*, *agp1Δ* and *gnp1Δagp1Δ* mutants as compared to WT cells (Fig 3a). As expected, the *gnp1Δ* strain showed a strong reduction (65%) in serine uptake compared to WT cells already 5 minutes after adding the labelled substrate (Fig 3a). Similarly, *agp1Δ* cells displayed a pronounced effect on serine uptake although substantially weaker than *gnp1Δ* cells with about 34% decrease in serine uptake compared to WT cells after 5 minutes. This observation is not reflected in our genetic analyses where Gnp1 appears to be responsible for most of the serine uptake and potentially represents a difference in the serine availability of the respective growth media. A strain lacking both,

198 *GNP1* and *AGP1,* showed almost no transport activity (Fig 3a). These results confirm that
199 Gnp1 is the major serine transporter in yeast under the used growth conditions.

200 Serine is a metabolic precursor in multiple pathways besides SP biosynthesis. Thus, it
201 is a donor of one-carbon units to folate (Ramos and Wiame, 1982), important for the synthesis
202 of GPLs such as phosphatidylserine [28,29] and phosphatidylethanolamine [30], and it is
203 required for protein synthesis. To test the effect of a *GNP1* deletion on protein biosynthesis,
204 we grew WT cells, *gnp1*Δ cells and *ser2*Δ cells in the presence of [$^{13}C_3{}^{15}N_1$]-serine and
205 measured its incorporation into proteins using mass spectrometry-based proteomics.
206 Extracted proteins were digested with the endo-proteinase Lys-C and only peptides containing
207 exactly one serine were analyzed. In WT cells 28% of the analyzed peptides contained a
208 [$^{13}C_3{}^{15}N_1$]- serine (Fig 3c). This suggests that either only a quarter of the intracellular serine is
209 imported or that the majority of the imported serine is directed towards metabolic pathways
210 other than protein biosynthesis. In line with the data reported above, only half of the [$^{13}C_3{}^{15}N_1$]-
211 serine was incorporated into proteins in *gnp1Δ* cells resulting in a reduction to a total of 14%
212 (Fig 3c). The remaining incorporation of [$^{13}C_3{}^{15}N_1$]-serine is probably due to serine uptake
213 mediated by Agp1. Interestingly, the serine auxotroph *ser2Δ* reached only an incorporation
214 rate of 56% (Fig 3c). This suggests that *ser2Δ* cells can still synthesize significant amounts of
215 serine, for example by the reverse action of the serine hydroxymethyltransferases Shm1 and
216 Shm2 from glycine [16]. However, this pool of serine appears to be too small to render the cells
217 serine prototroph. Again, these results confirm that Gnp1 is the major serine transporter in
218 yeast with only minor contributions of its paralog Agp1.

219 In the course of proteomics analyses of *gnp1Δ* cells we gained further evidence that
220 Gnp1 directly contributes to intracellular serine levels. We measured the entire proteome of
221 *gnp1Δ* cells compared to WT cells using stable isotope labelling by amino acids in cell culture
222 (SILAC; Ong et al., 2002) combined with mass spectrometry-based proteomics. Among the
223 2322 proteins quantified (Fig 3 – source data 1) we found an up-regulation of several metabolic
224 enzymes, with a prevalence in amino acid metabolic processes (according to GO term

analysis). Amongst these enzymes are the 3-phosphoglycerate dehydrogenase Ser3 catalyzing a rate limiting step in serine and glycine metabolism, as well as a subunit of the glycine decarboxylase Gcv1 (Fig 3d). Interestingly, the most down-regulated protein was the catabolic serine deaminase Cha1 (Fig 3d). Cha1 is under strong transcriptional control of the Cha4 transcription factor and is known to be upregulated by exogenous serine [19]. Together, this indicates that intracellular serine levels in *gnp1Δ* cells are decreased, and thus forces cells to adjust by reprogramming their metabolism.

Intracellular serine concentrations depend on serine uptake

To predict how serine biosynthesis and uptake are correlated, we used flux variability analysis (FVA) which allows a prediction of possible fluxes through a reconstructed metabolic network. First, we analyzed the contribution of cellular processes involving serine (Fig 4a). Our results highlighted the glycine hydroxymethyltransferases Shm1 and Shm2 as two main producers and consumers of serine within the cell, respectively (Fig 4a). Additionally, serine synthesis by the phosphoserine phosphatase Ser2 and uptake of external serine were identified as potential serine sources. To establish how serine uptake is determined by the relevant serine fluxes, we modelled the net flux through Ser2, Shm1 and Shm2 at varied serine uptake rates. According to the model, serine synthesis outweighs serine consumption only at low serine uptake rates (Fig 4b). At higher serine uptake rates, excess serine appears to be converted to glycine by Shm2. The flux prediction for the sum of Shm1 and Shm2 fluxes was not changed compared to the flux prediction including Ser2 (S5 Fig). Thus, the impact of the 3-phospho-glycerate pathway seems to be very low regarding total serine fluxes.

To test this model, we measured cellular amino acid concentrations by mass spectrometry. We used media without amino acids (except for serine where indicated) together with prototrophic WT and *gnp1Δ* cells. The amount of detected serine in WT cells was significantly increased by 67% in media containing serine compared to cells grown in the absence of serine. This indicates a pronounced effect of serine uptake on intracellular serine concentrations (Fig 4c). In contrast, serine levels in *gnp1Δ* cells with and without serine were

252 comparable to WT cells grown in the absence of serine. This suggests that intracellular serine
253 levels are directly depending on Gnp1 mediated serine uptake. This observation was also
254 reflected in detected glycine levels, which were 120% increased for WT cells grown in media
255 with serine compared to WT cells grown without serine (Fig 4c). In addition, glycine levels also
256 did not increase in *gnp1Δ* cells grown in the presence of serine. As there was no glycine in the
257 media, this indicates conversion of the transported serine to glycine as predicted by the FVA.

258 **Serine uptake by Gnp1 is important to maintain SP homeostasis**

259 To test if serine availability is important to maintain SP homeostasis, we next analyzed
260 the contribution of Gnp1-dependent serine uptake on SP metabolism. First, serial dilutions of
261 WT, *gnp1Δ*, *agp1Δ* and *gnp1Δagp1Δ* cells were spotted on different drop-out media in the
262 presence or absence of serine and myriocin. As expected, all strains grew well on all plates in
263 the absence of myriocin (Fig 5a). This also rules out any important role of Gnp1 and Agp1 in
264 serine biosynthesis. Interestingly, *gnp1Δ* cells showed strong growth defects after inhibition of
265 SP biosynthesis by myriocin, even under conditions were growth of WT cells was not affected
266 (Fig 5a). Thus, Gnp1-mediated serine uptake is essential under conditions of impaired SP
267 metabolism. In line with our genetic analyses and serine uptake assays, growth of *agp1Δ* cells
268 was not affected by the presence of myriocin, while an additive effect was observed in the
269 *gnp1Δagp1Δ* double mutant (Fig 5a). Confirming the initial results, all strains were highly
270 sensitive to myriocin in the absence of external serine (Fig 5a).

271 To exclude possible side effects of myriocin, we tested if the effect of myriocin can be
272 recovered by the addition of phytosphingosine (PHS). PHS, together with dihydrosphingosine
273 (DHS) is one of the two LCBs in yeast. Myriocin inhibits the synthesis of 3-
274 ketodihydrosphingosine, the short-lived precursor of LCBs (Fig 1c). We used serial dilutions to
275 test the effect of myriocin and PHS on WT, *gnp1Δ, agp1Δ* and *gnp1Δagp1Δ* cells. We found
276 that addition of 25 µM PHS recovered the growth deficiency of *gnp1Δ* cells at 0.5 µM myriocin
277 (Fig 5c), suggesting that there are no side effects of myriocin treatment.

Gnp1 is a general amino acid permease which was previously described to transport glutamine, leucine, threonine, cysteine, methionine and asparagine in addition to serine [17]. For this reason, we tested if the transport of the other amino acids affects the connection between Gnp1 and SP metabolism. We performed serial dilutions of prototrophic WT, *gnp1Δ*, *agp1Δ* and *gnp1Δagp1Δ* cells on media without amino acids (except of serine were indicated). Without serine in the media, *gnp1Δ* cells showed no increased sensitivity to myriocin compared to WT cells (Fig 5c). This indicated that the sensitivity of *gnp1Δ* cells to myriocin is induced by amino acids in the media. On plates containing serine and 1.5 µM myriocin *gnp1Δ* cells were slightly decreased in growth compared to WT cells (Fig 5c). However, this effect was not as pronounced as observed before (Fig 5a). The *gnp1Δagp1Δ* cells were highly decreased in growth on plates with serine and 1.5 µM myriocin (Fig 5c). Together, this indicates the presence of serine as the cause of sensitivity for *gnp1Δ* and *gnp1Δagp1Δ* cells to SP depletion and suggests no contribution of other transported amino acids. The difference in the sensitivity of *gnp1Δ* cells towards myriocin in media with amino acids (Fig 5a) and media without amino acids except of serine in the media (Fig 5c) could be a result of different expression levels of the two permeases Gnp1 and Agp1 in these media [32]. So far, we were not able to add a tag to Gnp1 to control the expression of the permease in different conditions. N- and C-terminal tagging as well as tagging of a cytosolic loop of the enzyme with different tags rendered the protein non-functional. This was verified by negative genetic interactions with *ser2Δ* in tetrad dissection analysis (S7a, b, c, d and e Fig). In addition, we were not able to detect Gnp1 and Agp1 levels with and without serine by mass spectrometry-based proteomics (S7f Fig). Nevertheless, the *agp1Δ* strain showed no sensitivity to myriocin in both experiments (Fig 5a and 5c). Additionally, the general sensitivity of the cells to myriocin was highly increased in the media without amino acids, consistent with our previous observations that the absence of serine increased the sensitivity towards SP depletion (Fig 5c).

In the next step, we asked if the observed connection between serine uptake and SP homeostasis results in other genetic interactions. As Lcb1 and Lcb2, the two catalytic subunits

of the SPT are essential; we used deletions of *ORM1* and *ORM2* as a read-out for genetic interactions of this step of SP biosynthesis. Orm1 and Orm2 are negative regulators of the SPT and release their inhibition after phosphorylation. Moreover, *orm1Δorm2Δ* strains were shown to have increased amounts of LCBs [7]. A *gnp1Δagp1Δ* strain mated with an *orm1Δorm2Δ* strain was therefore subjected to tetrad analysis. The *orm1Δorm2Δ* double mutants showed a growth defect, which was partly restored by the additional deletion of *GNP1,* but not by that of *AGP1.* The *orm1Δorm2Δgnp1Δagp1Δ* quadruple mutants showed the same growth defect as the triple mutants of *orm1Δorm2Δgnp1Δ,* again in line with Gnp1 being the major serine transporter under the tested conditions. The recovery of the growth defect by the deletion of *GNP1* indicates a rescue of increased SP levels due to decreased serine uptake. Together, this suggests a regulatory effect of serine uptake on SP metabolism.

To exclude a general effect of diminished serine uptake towards the SP biosynthesis pathway, we performed genetic interaction studies with additional enzymes of the SP biosynthesis pathway. None of the tested gene deletions (*sur2Δ*, *sur4Δ*, *lcb3Δ*, *lcb4Δ*, *scs7Δ*; see Fig 1c for an overview of the SP biosynthesis pathway) displayed a synthetic phenotype with *gnp1Δ* or *ser2Δ* (S8 Fig). This indicates a specific genetic interaction of Gnp1 with the first, serine-consuming step of SP biosynthesis.

To further substantiate these findings, we performed serial dilutions of WT, *gnp1Δ*, *agp1Δ* and *gnp1Δagp1Δ* cells on media containing the inhibitor Aureobasidin A, which blocks the formation of inositol-phosphorylceramides (IPCs). All tested strains showed comparable sensitivity to Aureobasidin A, indicating no interaction of serine uptake with this step of SP biosynthesis (S9a Fig). We also monitored the effect of fatty acid availability with Gnp1-mediated serine uptake by spotting WT, *gnp1*Δ, *agp1*Δ and *gnp1*Δ*agp1*Δ cells on plates containing cerulenin, an inhibitor of the fatty acid synthase. All tested strains (WT, *gnp1*Δ, *agp1*Δ and *gnp1*Δ*agp1*Δ) showed comparable growth defects, ruling out an effect of Gnp1 on palmitoyl-CoA availability (S9b Fig). All these results are in line with our genetic studies, indicating a prominent interaction of the first SP catalyzing step and serine uptake.

Gnp1-transported serine is the main source for sphingolipid biosynthesis

Finally, we decided to analyze the direct effect of serine uptake on yeast LCB levels as a readout of SPT activity. FVA predicted a direct relationship between increased SPT flux and increased serine uptake (Fig 6a). To experimentally test this connection, we measured PHS levels of WT and *gnp1Δ* cells under high and low concentrations of myriocin by LC-MS. It was previously shown that yeast cells can maintain constant levels of LCBs in the presence of low myriocin concentrations [7]. This was attributed to a negative feedback loop involving TORC2, Slm1/2 proteins, the Ypk kinases and the Orm proteins as negative regulators of the SPT [8,9,33]. At low myriocin concentrations, the SPT is partially inhibited, while the remaining SPT molecules are most likely upregulated by the described feedback mechanism, resulting in the tolerance of WT cells to low concentrations of myriocin (Fig 6c). Our analysis revealed that the *GNP1* deletion had no significant effect on PHS levels as compared to WT cells (Fig 6b). As expected, treatment with a high concentration of 100 ng myriocin per ml (0.25 µM) resulted in a strong depletion of PHS in WT and *gnp1Δ* cells (Fig 6b), suggesting that the cells are not able to compensate the inhibition of SP biosynthesis. However, treatment of the cells with 10 ng myriocin per ml (0.025 µM) resulted in only a small, non-significant decrease in PHS levels in WT cells confirming previous studies [7]. In contrast, PHS levels in *gnp1Δ* cells decreased significantly compared to equally treated WT cells (Fig 6b), suggesting a regulatory impact of serine uptake on SP metabolism.

To establish the correlation between extracellular serine uptake and SP metabolism more directly, we measured the incorporation of [$^{13}C_3{}^{15}N_1$]-serine and [$^{2}H_6$]-inositol into SPs. We labelled WT, *gnp1Δ*, *gnp1Δagp1Δ* and *ser2Δ* cells in duplicates for 90 minutes with [$^{13}C_3{}^{15}N_1$]-serine and [$^{2}H_6$]-inositol and measured their incorporation into the lipidome by high-resolution shotgun lipidomics. The analysis of [$^{13}C_3{}^{15}N_1$]-serine labelled IPCs revealed a 64% decrease in serine labelling in *gnp1Δ* cells and a decrease of 73% in *gnp1Δagp1Δ* cells compared to WT cells (Fig 6d). This effect was also observed in the detected ceramides (S13 Fig). The decreased serine labelling of SPs without Gnp1 and the low difference in labelling

between the *GNP1* deletion and the *GNP1 AGP1* deletion indicate Gnp1 again as the major serine permease in yeast. The results further demonstrate the integration of transported serine into SPs and thus the direct connection between serine uptake and SP metabolism. In addition, [$^2H_6$]-inositol labelled IPCs were slightly increased in *gnp1Δ* cells and in *gnp1Δagp1Δ* cells compared to WT cells, indicating perturbances in SP metabolism in the absence of serine uptake (Fig 6e).

In serine auxotrophic cells (*ser2Δ* cells) [$^{13}C_3{}^{15}N_1$]-serine and [$^2H_6$]-inositol labelled IPC levels remained in the same range as in WT cells (Figs 6d and 6e), pointing to the direct use of exogenous serine for *de novo* SP biosynthesis. If mainly serine synthesized by yeast cells would be used for SP metabolism, a decrease in labelling between WT cells and serine auxotrophic cells would be expected. Together, these results suggest a model in which Gnp1-transported serine is the main source of serine for the synthesis of SPs.

Discussion

Here we show that external serine uptake is crucial to maintain SP homeostasis in *S. cerevisiae.* We identify the broad-specificity amino acid permease Gnp1 as the main serine transporter in yeast. Loss of Gnp1 leads to a major reduction in serine uptake and renders the cells sensitive to chemical inhibition of SP biosynthesis. While LCB levels in *gnp1Δ* cells are relatively constant under normal growth conditions, the cells are unable to regulate SP biosynthesis according to need. Using metabolic flux analysis, we further show that *de novo* SP biosynthesis mainly depends on the uptake of extracellular serine by Gnp1 and its paralog Agp1. Together, these findings add serine uptake as another mechanism to maintain SP homeostasis in yeast.

Our data confirm previous studies that have found the overexpression of Gnp1 and Agp1 to result in increased uptake of serine [17]. In addition, it has been reported that heat stress results in the upregulation of SP biosynthesis. Serine for increased SP biosynthetic rates

385 is mainly taken from external sources [18]. This suggests that the cytosolic pools of serine are
386 not sufficient or spatially unavailable for increased SP biosynthesis rates. Intracellular serine
387 concentrations in yeast differ significantly across the literature [34,35]. In the experimental
388 conditions applied herein, the internal serine concentration is in the range of 3 to 6 nmol/10^8
389 cells. Since the majority of amino acids, including serine, are sequestered in the yeast vacuole
390 [36,37], this pool of serine would not be available for SP biosynthesis. This could be especially
391 important under conditions where yeast has to synthesize large amounts of SPs in a short
392 time. Thus, it is a very interesting model that serine uptake is directly coupled to *de novo* SP
393 biosynthesis by the SPT (Fig 7).

394 The SPOTS complex (SPT, Orm1/2, Tsc3, and Sac1) is present in both, the nuclear as
395 well as the cortical ER of yeast cells [7,38]. The cortical ER has recently been shown to be
396 closely associated with the plasma membrane in ER-membrane contact sites [39,40]. Thus,
397 Gnp1-mediated serine uptake could be directly coupled to SP biosynthesis. Besides all efforts,
398 we were so far unable to localize a functional Gnp1 construct in cells. Thus, it remains open,
399 if Gnp1 co-localizes with the SPOTS complex of the cortical ER.

400 Amongst other mechanisms, SPT is negatively regulated by phosphorylation of the
401 associated Orm proteins [7]. This signaling cascade starts at the plasma membrane with the
402 re-localization of the Slm1/2 proteins to the TOR complex 2 and subsequent phosphorylation
403 of the Ypk1 kinase, which then phosphorylates the Orm proteins [8,9]. The exact mechanism
404 that leads to upregulation of SPT activity after Orm phosphorylation is still not clear, but recent
405 data suggest that phosphorylated Orm2 is transported to the Golgi and degraded by the
406 endosome-Golgi associated degradation (EGAD) pathway [38]. Since TORC2 and the Ypk
407 kinases are located at the plasma membrane [8,10] it seems likely that downstream effectors,
408 such as the SPOTS complex, are also located in close proximity. In this model, two pools of
409 SPT are present in the cells i) a pool localized at the nuclear envelope that is responsible for
410 constant SP biosynthesis and ii) a pool that can be actively regulated to synthesize large
411 amounts of SPs according to need (Fig 7). In addition, this model could also be an explanation
412 of the different behavior of Orm1 and Orm2. While Orm2 appears to be a target of the EGAD

pathway and is mainly regulated by Ypk1, Orm1 seems to be mainly regulated via the Npr1 kinase, via the TOR complex 1 signaling pathway [9,38]. However, data obtained from our metabolic flux analysis suggest that external serine is the main source for SP biosynthesis.

In summary, we propose a model where the upregulation of the SPT is directly coupled to nutrient uptake, most likely at ER/plasma membrane contact sites (Fig 7). This system could work similar to other processes where the uptake/release of a small molecule is directly coupled to downstream pathways. One such example is local calcium dynamics at ER/mitochondria contact sites [41]. Another example where substrate availability is directly coupled to a downstream process is the recently described fatty acid channeling into phospholipid biosynthetic enzymes at sites of autophagosome formation [42]. In any case, our model would also require direct regulation of Gnp1. This could be achieved by manipulating the abundance of Gnp1 via regulated biosynthesis or degradation, or by regulating its transport activity by post-translational modifications. Gnp1 mRNA was shown to be regulated by the Ssy1p–Ptr3p–Ssy5 (SPS) sensor of extracellular amino acids upon the addition of leucine [43]. Yet, we did not detect changes in Gnp1 abundance by proteomics experiments in response to serine depletion (S7e Fig and S12). As an alternative regulatory mechanism, we have previously identified a phosphorylation site at serine 124 of Gnp1 after myriocin treatment, indicating its regulation in response to SP depletion [14]. In addition, Gnp1 is differentially phosphorylated in response to the TORC1 inhibitor rapamycin in *npr1Δ* cells. Npr1 has been shown to regulate plasma membrane proteins by regulated endocytosis via the arrestin proteins [44–46]. Thus, it is interesting to speculate that Gnp1 could be affected by TORC1, which has also been linked to SP homeostasis [47]. Interestingly, the genetic data presented herein also revealed synthetic phenotypes with multiple components of the TORC1 in serine auxotroph cells (S1). Testing this hypothesis will require functional fluorescent tags of Gnp1 for cell biological and biochemical approaches, whose construction failed so far.

Varying extracellular serine concentrations have been linked to SP metabolism in mammalian cells [48,49]. Therefore, it is possible that salient features of the serine uptake-SP regulatory system are also conserved. While Gnp1 does not have a clear homolog in

mammalian cells, ASCT1 has been identified as a serine transporter in brain cells [50]. Interestingly, mutations in the brain serine transporter ASCT1 (Slc1a4) have been linked to neurodevelopmental/neurodegenerative disorders [51,52]. Although no changes in SP levels were observed in ASCT1 knockout mice so far, this could be explained by the sole determination of steady state SP levels in these studies [53]. In another neurological condition, HSNA1 (hereditary sensory and autonomic neuropathy 1), mutations in SPT result in the incorporation of alanine yielding desoxy-SPs [41]. Interestingly, high dose oral serine supplementation appears to have positive effects on patients, suggesting a functional serine uptake in their cells [54,55]. While the regulation of SP homeostasis by the ORMDL proteins in mammalian cells still remains mechanistically poorly understood, the components we identified in the yeast system are generally also present in mammalian cells. Thus, the coupling of serine uptake and SP homeostasis might be evolutionary conserved.

Materials and Methods

Yeast strains and plasmids

Yeast strains used in this study are listed in Table 1. Serine metabolism knockout strains were from the yeast deletion collection [21]. All tetrad analysis experiments were performed in the W303 strain background. All other experiments including serine uptake assays, proteomics and lipidomics experiments were performed in the SEY6210 background.

Yeast media and growth conditions

Tetrad dissections were performed on standard YPD plates. To generate a synthetic medium (SDC) with or without serine we used 6.7 g/l yeast nitrogen base, 20 g/l glucose and self-made drop out mix consisting of 20 mg/l adenine; 60 mg/l leucine; 20 mg/l alanine; 100 mg/l aspartic acid; 100 mg/l glutamic acid; 20 mg/l histidine; 30 mg/l isoleucine; 30 mg/l lysine; 20 mg/l methionine; 50 mg/l phenylalanine; 200 mg/l threonine; 20 mg/l tryptophan; 30 mg/l tyrosine; 20 mg/l uracil and 150 mg/l valine. To generate synthetic medium without amino acids we used

6.75 g/l yeast nitrogen base and 20 g/l glucose. Serine was added where indicated to a final concentration of 400 mg/l.

For serine incorporation measurements into proteins, cells were grown in SDC (see dropout mix above) containing 400 mg/l [$^{13}C_3{}^{15}N_1$]-serine overnight for at least 15 doublings.

For SILAC labeling, lysine auxotrophic strains SEY6210 and FFY727 were grown in SDC medium containing the same dropout mix with either 30 mg/L lysine (SEY6210) or 30 mg/L [$^{13}C_6{}^{15}N_2$]-lysine (FFY727) to OD_{600}=0.7 for at least 15 generation times to ensure full labeling.

Spotting assays

For spotting assays, cells were grown to exponential growth phase and serial diluted. Cells were spotted on the corresponding plates and incubated at 30 °C for three days. YPD and SD media with and without amino acids were used as indicated. Chemicals were added in the indicated concentrations.

Serine uptake assays

Amino acid uptake assays were performed as previously described [56] with minor modifications. Briefly, WT, *gnp1Δ*, *agp1Δ* and *gnp1Δagp1Δ* cells were grown in synthetic medium with serine for at least 13 doublings to reach an OD_{600}=0.5. With the aid of a vacuum system, cells were filtered and resuspended from the filters (MF^{TM} Membrane Filters 0.45 µm, Merck KGaA, 64293 Darmstadt, Germany) in the same volume of synthetic medium without serine. OD_{600} was measured and 0.72 mM [^{14}C]-serine were added. At 5, 15 and 30 min 1 ml of the culture was filtered with serine-saturated filters. To measure the background 1 ml of the 0.72 mM [^{14}C]-serine solution was also filtered the same way. The filters were covered by a scintillation liquid and the radioactivity was measured with a scintillation counter (Beckman Coulter LS 6500 Multi-Purpose Scintillation Counter, GMI Trusted Laboratory Solutions, MN 55303, USA). The transport was expressed as nmol/mg of protein per unit of time and reported as the mean ± S.D. (n = 3).

Proteomics

Proteomics analysis was performed as described previously [57]. Briefly, yeast cells were lysed using the filter aided sample preparation method [58]. For full proteome analysis, samples were eluted from a PepMap C18 easy spray column (Thermo) with a linear gradient of acetonitrile from 10–35% in H_2O with 0.1% formic acid for 118 min at a constant flow rate of 300 nl/min.

For serine incorporation assays using [$^{13}C_3{}^{15}N_1$]-serine (Cambridge Isotope Labs) samples were eluted from a PepMap C18 easy spray column (Thermo) with a linear gradient of acetonitrile from 10–50% in 0.1% formic acid for 33 min at a constant flow rate of 300 nl/min.

The resulting MS and MS/MS spectra were analyzed using MaxQuant (version 1.6.0.13, www.maxquant.org/; Cox et al., 2011; Cox and Mann, 2008) as described previously [57]. For incorporation tests, [$^{13}C_3{}^{15}N_1$]-serine was added as a modification to the MaxQuant database (mass change =4.0070994066 Da). For the calculation of incorporation rates, the peptide list was filtered for serine containing peptides with a valid heavy/light ratio. For each peptide, the incorporation was calculated as 1 - (1/(ratio H/L - 1)). The maximum of a density distribution of all peptides represents the estimated incorporation level. All calculations and plots were performed with the R software package (www.r-project.org/; RRID:SCR_001905).

LCB Analysis

For LC-MS analysis of LCBs, cells were grown in YPD to exponential growth phase and labelled for 3 hours with the indicated concentrations of myriocin. Lipids were extracted from lysed yeast cells according to 50 µg of protein by chloroform/methanol extraction [61]. Prior to extraction sphingosine (LCB 17:0) was spiked into each sample for normalization and quantification. Dried lipid samples were dissolved in a 65:35 mixture of mobile phase A (60:40 water/acetonitrile, including 10 mM ammonium formate and 0.1% formic acid) and mobile phase B (88:10:2 2-propanol/acetonitrile/H_20, including 2 mM ammonium formate and 0.02% formic acid). HPLC analysis was performed on a C30 reverse-phase column (Thermo Acclaim C30, 2.1 × 250 mm, 3 µm, operated at 50°C; Thermo Fisher Scientific) connected to an HP 1100 series HPLC (Agilent) HPLC system and a QExactive*PLUS* Orbitrap mass spectrometer

(Thermo Fisher Scientific) equipped with a heated electrospray ionization (HESI) probe. The analysis was performed as described previously [62]. Peaks were analyzed using the Lipid Search algorithm (MKI, Tokyo, Japan). Peaks were defined through raw files, product ion and precursor ion accurate masses. Candidate molecular species were identified by database (>1,000,000 entries) search of positive ($+H^+$) ion adducts. Mass tolerance was set to five ppm for the precursor mass. Samples were aligned within a time window 0.5 min and results combined in a single report. From the intensities of the lipid standard absolute values for each lipid in pmol/mg protein were calculated. Data are displayed as fold change from WT.

Quantification of cellular amino acids

Prototroph strains were grown in synthetic medium without amino acids (except of the addition of serine were indicated), collected by centrifugation and washed with ice-cold H_20 for three times. Cell lysis and amino acid extractions were performed following the modified protocol from Mülleder et al., 2016. Ethanol containing the non-proteinogeneic amino acid norleucin was added to the pellet, mixed and heated to 80° C for 5 minutes. The extract was sonicated for 15 minutes and the heating step was repeated. The extract was cleared by centrifugation, dried and resolved in H_20 with 10% acetonitrile. The amino acids were derivatized with dansyl-chloride and analysed by LC-MS/MS.

Amino acids were separated by hydrophilic interaction liquid chromatography using a Shimadzu Nexera HPLC with ThermoFisher Accurore RP-MS C18 column (0.21 x 150 mm; 2.6 µm particle size). For the mobile phases 0.1% formic acid in water (A) and 0.1% formic acid in 80% acetonitrile (B) was used. For the gradient 0 to 50% B over 0.7 min, 50% to 60% over 3.7 min, 60% to 100% B over 0.1 min, 100% B kept for 0.5min and 0% B for 1.5 min and a constant flow rate of 0.4 ml/min was used with a total analysis time of 6 minutes and an injection volume of 1 µl. The samples were analyzed by a QTRAP® 5500 LC-MS/MS system (SCIEX), with IonDrive™ TurboV source. The MS data were acquired in positive, scheduled MRM mode with 20 sec detection windows (Gly: Q1 309, Q3 170, RT 2.65min, DP 111V, CE, 27V, CXP 26V; Ser: Q1 339, Q3 170, RT 2.02min, DP 36V, CE, 29V, CXP 6V). For peak

integration SciexOS™ software was used. The Amino Acid Standard H from Thermo Fischer was used to quantify the amino acids. The amino acid concentrations were expressed in nmol per 10^8 cells and reported as the mean ± S.D. (n = 3).

Modelling flux variability

Flux variability analysis (FVA) [63] was performed on the yeast consensus genome-scale model yeast-GEM-v7.6.0 [64] and constraints were adjusted to simulate growth in SDC medium and to account for the gene deletions in the SEY6210 mutant. The computed minimum and maximum fluxes correspond to the solution space which supports 99 % of maximum feasible biomass growth. We used COBRA Toolbox v3.0 [65] in MATLAB (The MathWorks, Inc.) and employed the algorithm fastFVA [66] and CPLEX 12.8 (IBM Corp.) to solve optimization problems. The metabolic model is available at https://github.com/SysBioChalmers/yeast-GEM/tree/v7.6.0. Our MATLAB script is provided in S9 Script.

Lipidomics flux analysis

Yeast strains were pre-cultured in YPD. At an OD_{600} of 0.8, 5 ml cell suspensions were spiked with a tracer cocktail resulting in final concentrations of 4.59 mM [$^{13}C_3{}^{15}N_1$]-serine and 0.22 mM [$^2H_6$]-inositol. After 90 minutes, the cell suspensions were incubated at 4 °C for 10 min with 1M perchloric acid. The cells were centrifuged and washed with 4 ºC 155 mM ammonium formate, frozen in liquid nitrogen and stored at –80 ºC.

In-depth lipidome analysis was performed as described previously [67,68]. In short, yeast cell pellets (~5 ODunits) were resuspended in 1 ml of 155 mM ammonium formate and lysed at 4 °C with 400 µl of acid-washed glass beads using a Mini-Beadbeater (Biospec). Lysates corresponding with 0.4 OD units were subsequently spiked with internal lipid standards and subjected to two-step lipid extraction [68]. Lipid extracts were vacuum evaporated and re-dissolved in 100 µl chloroform/methanol (1:2; v/v) and analyzed by MS^{ALL} [69] using an Orbitrap Fusion Tribrid (Thermo Fisher Scientific) equipped with a TriVersa NanoMate robotic nanoflow

ion source (Advion Biosciences). Lipid identification and quantification was done using ALEX^{123} software [70–72]. The results were expressed in mol % per all detected lipids (n = 2).

Acknowledgments

We thank members of the Fröhlich lab for critical comments on the manuscript.

References

1. Van Meer G, Voelker DR, Feigenson GW. Membrane lipids: Where they are and how they behave. Nat Rev Mol Cell Biol. 2008;9: 112–124. doi:10.1038/nrm2330

2. Dickson RC, Lester RL. Yeast sphingolipids. Biochim Biophys Acta - Gen Subj. 1999;1426: 347–357. doi:10.1016/S0304-4165(98)00135-4

3. Hanada K, Kumagai K, Yasuda S, Miura Y, Kawano M, Fukasawa M, et al. Molecular machinery for non-vesicular trafficking of ceramide. Nature. 2003;426: 803–809. doi:10.1038/nature02188

4. Liu LK, Choudhary V, Toulmay A, Prinz WA. An inducible ER-Golgi tether facilitates ceramide transport to alleviate lipotoxicity. J Cell Biol. 2017;216: 131–147. doi:10.1083/jcb.201606059

5. Klemm RW, Ejsing CS, Surma MA, Kaiser HJ, Gerl MJ, Sampaio JL, et al. Segregation of sphingolipids and sterols during formation of secretory vesicles at the trans-Golgi network. J Cell Biol. 2009. doi:10.1083/jcb.200901145

6. Heinisch JJ, Rodicio R. Protein kinase C in fungi—more than just cell wall integrity. FEMS Microbiol Rev. 2018;42. doi:10.1093/femsre/fux051

7. Breslow DK, Collins SR, Bodenmiller B, Aebersold R, Simons K, Shevchenko A, et al. Orm family proteins mediate sphingolipid homeostasis. Nature. 2010;463: 1048–1053. doi:10.1038/nature08787

8. Berchtold D, Piccolis M, Chiaruttini N, Riezman I, Riezman H, Roux A, et al. Plasma

membrane stress induces relocalization of Slm proteins and activation of TORC2 to promote sphingolipid synthesis. Nat Cell Biol. 2012;14: 542–547. doi:10.1038/ncb2480

9. Roelants FM, Breslow DK, Muir A, Weissman JS, Thorner J. Protein kinase Ypk1 phosphorylates regulatory proteins Orm1 and Orm2 to control sphingolipid homeostasis in Saccharomyces cerevisiae. Proc Natl Acad Sci U S A. 2011;108: 19222–7. doi:10.1073/pnas.1116948108

10. Muir A, Ramachandran S, Roelants FM, Timmons G, Thorner J. TORC2-dependent protein kinase Ypk1 phosphorylates ceramide synthase to stimulate synthesis of complex sphingolipids. Elife. 2014;3: 1–34. doi:10.7554/eLife.03779

11. Fröhlich F, Moreira K, Aguilar PS, Hubner NC, Mann M, Walter P, et al. A genome-wide screen for genes affecting eisosomes reveals Nce102 function in sphingolipid signaling. J Cell Biol. 2009;185: 1227–1242. doi:10.1083/jcb.200811081

12. Olson DK, Fröhlich F, Christiano R, Hannibal-bach HK, Ejsing CS, Walther TC. Rom2-dependent Phosphorylation of Elo2 Controls the Abundance of Very Long-chain Fatty Acids * □. J Biol Chem. 2015;290: 4238–4247. doi:10.1074/jbc.M114.629279

13. Zimmermann C, Santos A, Gable K, Epstein S, Gururaj C, Chymkowitch P, et al. TORC1 Inhibits GSK3-Mediated Elo2 Phosphorylation to Regulate Very Long Chain Fatty Acid Synthesis and Autophagy. Cell Rep. 2013;5: 1036–1046. doi:10.1016/J.CELREP.2013.10.024

14. Fröhlich F, Olson DK, Christiano R, Farese R V., Walther TC. Proteomic and phosphoproteomic analyses of yeast reveal the global cellular response to sphingolipid depletion. Proteomics. 2016;16: 2759–2763. doi:10.1002/pmic.201600269

15. Albers E, Laizé V, Blomberg A, Hohmann S, Gustafsson L. Ser3p (Yer081wp) and Ser33p (Yil074cp) are phosphoglycerate dehydrogenases in Saccharomyces cerevisiae. J Biol Chem. 2003;278: 10264–10272. doi:10.1074/jbc.M211692200

624 16. Kastanos EK, Woldman YY, Appling DR. Role of mitochondrial and cytoplasmic serine
625 hydroxymethyltransferase isozymes in de Novo purine synthesis in Saccharomyces
626 cerevisiae. Biochemistry. 1997;36: 14956–14964. doi:10.1021/bi971610n

627 17. Regenberg B, Düring-Olsen L, Kielland-Brandt MC, Holmberg S. Substrate specificity
628 and gene expression of the amino-acid permeases in Saccharomyces cerevisiae. Curr
629 Genet. 1999;36: 317–328. doi:10.1007/s002940050506

630 18. Cowart LA, Hannun YA. Selective substrate supply in the regulation of yeast de novo
631 sphingolipid synthesis. J Biol Chem. 2007;282: 12330–12340.
632 doi:10.1074/jbc.M700685200

633 19. Montefusco DJ, Newcomb B, Gandy JL, Brice SE, Matmati N, Cowart LA, et al.
634 Sphingoid bases and the serine catabolic enzyme CHA1 define a novel
635 feedforward/feedback mechanism in the response to serine availability. J Biol Chem.
636 2012;287: 9280–9. doi:10.1074/jbc.M111.313445

637 20. Gournas C, Prévost M, Krammer EM, André B. Function and regulation of fungal
638 amino acid transporters: Insights from predicted structure. Advances in Experimental
639 Medicine and Biology. Springer, Cham; 2016. pp. 69–106. doi:10.1007/978-3-319-
640 25304-6_4

641 21. Winzeler EA, Astromoff A, Liang H, Anderson K, Andre B, Bangham R, et al.
642 Functional Characterization of the S. cerevisiae Genome by Gene deletion and
643 Parallel Analysis. Science (80-). 1999;285: 901–906. Available:
644 http://science.sciencemag.org/

645 22. Ulane R, Ogur M. Genetic and physiological control of serine and glycine biosynthesis
646 in Saccharomyces. J Bacteriol. 1972;109: 34–43.

647 23. Fröhlich F, Petit C, Kory N, Christiano R, Hannibal-Bach HK, Graham M, et al. The
648 GARP complex is required for cellular sphingolipid homeostasis. Elife. 2015;4.
649 doi:10.7554/eLife.08712

650 24. Wadsworth JM, Clarke DJ, McMahon SA, Lowther JP, Beattie AE, Langridge-Smith
651 PRR, et al. The Chemical Basis of Serine Palmitoyltransferase Inhibition by Myriocin. J
652 Am Chem Soc. 2013;135: 14276–14285. doi:10.1021/ja4059876

653 25. Costanzo M, Baryshnikova A, Bellay J, Kim Y, Spear ED, Sevier CS, et al. The genetic
654 landscape of a cell. Science (80-). 2010;327: 425–431. doi:10.1126/science.1180823

655 26. Byrne KP, Wolfe KH. The Yeast Gene Order Browser: combining curated homology
656 and syntenic context reveals gene fate in polyploid species. Genome Res. 2005;15:
657 1456–61. doi:10.1101/gr.3672305

658 27. RAMOS F, WIAME J -M. Occurrence of a Catabolic l-Serine (l-Threonine) Deaminase
659 in Saccharomyces cerevisiae. Eur J Biochem. 1982;123: 571–576. doi:10.1111/j.1432-
660 1033.1982.tb06570.x

661 28. Bae-lee MS, Carman GM. Phosphatidylserine Synthesis in Saccharomyces
662 cerevisiae. Society. 1984;259: 10857–10862. Available:
663 http://eutils.ncbi.nlm.nih.gov/entrez/eutils/elink.fcgi?dbfrom=pubmed&id=6088519&ret
664 mode=ref&cmd=prlinks%5Cnpapers2://publication/uuid/2D4A67C9-3F3D-4BE2-9378-
665 80D09EA33EAB

666 29. Kanfer J, Kennedy EP. Metabolism and Function of Bacterial Lipids. J Biol Chem.
667 1964;239: 1720–1727.

668 30. Summers EF, Letts VA, McGraw P, Henry SA. Saccharomyces cerevisiae cho2
669 mutants are deficient in phospholipid methylation and cross-pathway regulation of
670 inositol synthesis. Genetics. 1988;120: 909–922.

671 31. Ong S-E, Blagoev B, Kratchmarova I, Kristensen DB, Steen H, Pandey A, et al. Stable
672 isotope labeling by amino acids in cell culture, SILAC, as a simple and accurate
673 approach to expression proteomics. Mol Cell Proteomics. 2002;1: 376–86.
674 doi:10.1074/MCP.M200025-MCP200

675 32. Forsberg H, Gilstring CF, Zargari A, Martínez P, Ljungdahl PO. The role of the yeast

plasma membrane SPS nutrient sensor in the metabolic response to extracellular amino acids. Mol Microbiol. 2008;42: 215–228. doi:10.1046/j.1365-2958.2001.02627.x

33. Han S, Lone MA, Schneiter R, Chang A. Orm1 and Orm2 are conserved endoplasmic reticulum membrane proteins regulating lipid homeostasis and protein quality control. Proc Natl Acad Sci U S A. 2010;107: 5851–5856. doi:10.1073/pnas.0911617107

34. Lee JCY, Tsoi A, Kornfeld GD, Dawes IW. Cellular responses to <scp>L</scp> -serine in *Saccharomyces cerevisiae* : roles of general amino acid control, compartmentalization, and aspartate synthesis. FEMS Yeast Res. 2013;13: 618–634. doi:10.1111/1567-1364.12063

35. Mülleder M, Calvani E, Alam MT, Wang RK, Eckerstorfer F, Zelezniak A, et al. Functional Metabolomics Describes the Yeast Biosynthetic Regulome. Cell. 2016;167: 553-565.e12. doi:10.1016/j.cell.2016.09.007

36. Klionsky DJ, Herman PK, Emr SD. The Fungal Vacuole: Composition, Function, and Biogenesis. Microbiol Rev. 1990. Available: http://mmbr.asm.org/

37. Kitamoto K, Yoshizawa K, Ohsumi Y, Anraku2 Y. Dynamic Aspects of Vacuolar and Cytosolic Amino Acid Pools of Saccharomyces cerevisiae. J Bacteriol. 1988. Available: http://jb.asm.org/

38. Schmidt O, Weyer Y, Baumann V, Widerin MA, Eising S, Angelova M, et al. Endosome and Golgi-associated degradation (<scp>EGAD</scp>) of membrane proteins regulates sphingolipid metabolism. EMBO J. 2019;38. doi:10.15252/embj.2018101433

39. Collado J, Kalemanov M, Martinez-Sanchez A, Campelo F, Baumeister W, Stefan CJ, et al. Tricalbin-Mediated Contact Sites Control ER Curvature to Maintain Plasma Membrane Integrity. SSRN Electron J. 2019; 476–487. doi:10.2139/ssrn.3371409

40. Hoffmann PC, Wozny MR, Boulanger J, Miller EA, Kukulski W, Hoffmann PC, et al. Tricalbins Contribute to Cellular Lipid Flux and Form Curved ER-PM Contacts that Are

Bridged by Rod- Article Tricalbins Contribute to Cellular Lipid Flux and Form Curved ER-PM Contacts that Are Bridged by Rod-Shaped Structures. Dev Cell. 2019;51: 488-502.e8. doi:10.1016/j.devcel.2019.09.019

41. Csordás G, Várnai P, Golenár T, Roy S, Purkins G, Schneider TG, et al. Imaging Interorganelle Contacts and Local Calcium Dynamics at the ER-Mitochondrial Interface. Mol Cell. 2010;39: 121–132. doi:10.1016/j.molcel.2010.06.029

42. Schütter M, Giavalisco P, Brodesser S, Graef M. Local Fatty Acid Channeling into Phospholipid Synthesis Drives Phagophore Expansion during Autophagy. Cell. 2020;180: 135-149.e14. doi:10.1016/j.cell.2019.12.005

43. Iraqui I, Vissers S, Bernard F, de Craene J-O, Boles E, Urrestarazu A, et al. Amino Acid Signaling in Saccharomyces cerevisiae : a Permease-Like Sensor of External Amino Acids and F-Box Protein Grr1p Are Required for Transcriptional Induction of the AGP1 Gene, Which Encodes a Broad-Specificity Amino Acid Permease . Mol Cell Biol. 1999;19: 989–1001. doi:10.1128/mcb.19.2.989

44. MacGurn JA, Hsu P-C, Smolka MB, Emr SD. TORC1 Regulates Endocytosis via Npr1-Mediated Phosphoinhibition of a Ubiquitin Ligase Adaptor. Cell. 2011;147: 1104–1117. doi:10.1016/j.cell.2011.09.054

45. Merhi A, Andre B. Internal Amino Acids Promote Gap1 Permease Ubiquitylation via TORC1/Npr1/14-3-3-Dependent Control of the Bul Arrestin-Like Adaptors. Mol Cell Biol. 2012;32: 4510–4522. doi:10.1128/mcb.00463-12

46. Gournas C, Saliba E, Krammer EM, Barthelemy C, Prévost M, André B. Transition of yeast Can1 transporter to the inward-facing state unveils an α-arrestin target sequence promoting its ubiquitylation and endocytosis. Mol Biol Cell. 2017;28: 2819–2832. doi:10.1091/mbc.E17-02-0104

47. Shimobayashi M, Oppliger W, Moes S, Jenö P, Hall MN. TORC1-regulated protein kinase Npr1 phosphorylates Orm to stimulate complex sphingolipid synthesis. Riezman H, editor. Mol Biol Cell. 2013;24: 870–881. doi:10.1091/mbc.e12-10-0753

729 48. Merrill AH, Wang E, Mullins RE. Kinetics of long-chain (sphingoid) base biosynthesis
730 in intact LM cells: effects of varying the extracellular concentrations of serine and fatty
731 acid precursors of this pathway. Biochemistry. 1988;27: 340–345.
732 doi:10.1021/bi00401a051

733 49. Gao X, Lee K, Reid MA, Li S, Liu J, Correspondence JWL. Serine Availability
734 Influences Mitochondrial Dynamics and Function through Lipid Metabolism. Cell Rep.
735 2018;22: 3507–3520. doi:10.1016/j.celrep.2018.03.017

736 50. Yamamoto T, Nishizaki I, Nukada T, Kamegaya E, Furuya S, Hirabayashi Y, et al.
737 Functional identification of ASCT1 neutral amino acid transporter as the predominant
738 system for the uptake of L-serine in rat neurons in primary culture. Neurosci Res.
739 2004. doi:10.1016/j.neures.2004.02.004

740 51. Damseh N, Simonin A, Jalas C, Picoraro JA, Shaag A, Cho MT, et al. Mutations in
741 SLC1A4, encoding the brain serine transporter, are associated with developmental
742 delay, microcephaly and hypomyelination. J Med Genet. 2015;1: 541–547.
743 doi:10.1136/jmedgenet-2015-103104

744 52. Heimer G, Marek-Yagel D, Eyal E, Barel O, Oz Levi D, Hoffmann C, et al. SLC1A4
745 mutations cause a novel disorder of intellectual disability, progressive microcephaly,
746 spasticity and thin corpus callosum. Clin Genet. 2015;88: 327–335.
747 doi:10.1111/cge.12637

748 53. Kaplan E, Zubedat S, Radzishevsky I, Valenta AC, Rechnitz O, Sason H, et al. ASCT1
749 (Slc1a4) transporter is a physiologic regulator of brain D-serine and
750 neurodevelopment. 2018;5. doi:10.1073/pnas.1722677115

751 54. Auranen M, Toppila J, Suriyanarayanan S, Lone MA, Paetau A, Tyynismaa H, et al.
752 Clinical and metabolic consequences of L-serine supplementation in hereditary
753 sensory and autonomic neuropathy type 1C. Cold Spring Harb Mol case Stud. 2017;3.
754 doi:10.1101/mcs.a002212

755 55. Fridman V, Suriyanarayanan S, Novak P, David W, Macklin EA, McKenna-Yasek D, et

al. Randomized trial of l -serine in patients with hereditary sensory and autonomic neuropathy type 1. Neurology. 2019;92: E359–E370. doi:10.1212/WNL.0000000000006811

56. Ghaddar K, Krammer E-M, Mihajlovic N, Brohée S, André B, Prévost M. Converting the yeast arginine can1 permease to a lysine permease. J Biol Chem. 2014;289: 7232–46. doi:10.1074/jbc.M113.525915

57. Fröhlich F, Christiano R, Walther TC. Native SILAC: metabolic labeling of proteins in prototroph microorganisms based on lysine synthesis regulation. Mol Cell Proteomics. 2013;12: 1995–2005. Available: http://www.ncbi.nlm.nih.gov/pubmed/23592334

58. Wiśniewski JR, Zougman A, Nagaraj N, Mann M. Universal sample preparation method for proteome analysis. Nat Methods. 2009;6: 359–62. doi:10.1038/nmeth.1322

59. Cox J, Mann M. MaxQuant enables high peptide identification rates, individualized p.p.b.-range mass accuracies and proteome-wide protein quantification. Nat Biotechnol. 2008;26: 1367–72. doi:10.1038/nbt.1511

60. Cox J, Neuhauser N, Michalski A, Scheltema RA, Olsen J V., Mann M. Andromeda: A peptide search engine integrated into the MaxQuant environment. J Proteome Res. 2011;10: 1794–1805. doi:10.1021/pr101065j

61. Ejsing CS, Sampaio JL, Surendranath V, Duchoslav E, Ekroos K, Klemm RW, et al. Global analysis of the yeast lipidome by quantitative shotgun mass spectrometry. Proc Natl Acad Sci U S A. 2009;106: 2136–41. doi:10.1073/pnas.0811700106

62. Eising S, Thiele L, Fröhlich F. A Systematic Approach to Identify Recycling Endocytic Cargo Depending on the GARP Complex Abstract. Elife. 2019.

63. Mahadevan R, Schilling CH. The effects of alternate optimal solutions in constraint-based genome-scale metabolic models. Metab Eng. 2003;5: 264–276. doi:10.1016/j.ymben.2003.09.002

64. Aung HW, Henry SA, Walker LP. Revising the representation of fatty acid, glycerolipid,

and glycerophospholipid metabolism in the consensus model of yeast metabolism. Ind Biotechnol. 2013;9: 215–228. doi:10.1089/ind.2013.0013

65. Heirendt L, Arreckx S, Pfau T, Mendoza SN, Richelle A, Heinken A, et al. Creation and analysis of biochemical constraint-based models using the COBRA Toolbox v.3.0. Nat Protoc. 2019;14: 639–702. doi:10.1038/s41596-018-0098-2

66. Gudmundsson S, Thiele I. Computationally efficient flux variability analysis. BMC Bioinformatics. 2010;11: 10–12. doi:10.1186/1471-2105-11-489

67. Almeida R, Pauling JK, Sokol E, Hannibal-Bach HK, Ejsing CS. Comprehensive lipidome analysis by shotgun lipidomics on a hybrid quadrupole-orbitrap-linear ion trap mass spectrometer. J Am Soc Mass Spectrom. 2015;26: 133–48. doi:10.1007/s13361-014-1013-x

68. Ejsing CS, Sampaio JL, Surendranath V, Duchoslav E, Ekroos K, Klemm RW, et al. Global analysis of the yeast lipidome by quantitative shotgun mass spectrometry. Proc Natl Acad Sci U S A. 2009;106: 2136–41. doi:10.1073/pnas.0811700106

69. Almeida R, Berzina Z, Arnspang EC, Baumgart J, Vogt J, Nitsch R, et al. Quantitative spatial analysis of the mouse brain lipidome by pressurized liquid extraction surface analysis. Anal Chem. 2015;87: 1749–1756. doi:10.1021/ac503627z

70. Ellis SR, Paine MRL, Eijkel GB, Pauling JK, Husen P, Jervelund MW, et al. Automated, parallel mass spectrometry imaging and structural identification of lipids. Nat Methods. 2018;15: 515–518. doi:10.1038/s41592-018-0010-6

71. Pauling JK, Hermansson M, Hartler J, Christiansen K, Gallego SF, Peng B, et al. Proposal for a common nomenclature for fragment ions in mass spectra of lipids. PLoS One. 2017;12. doi:10.1371/journal.pone.0188394

72. Husen P, Tarasov K, Katafiasz M, Sokol E, Vogt J, Baumgart J, et al. Analysis of lipid experiments (ALEX): A software framework for analysis of high-resolution shotgun lipidomics data. PLoS One. 2013;8. doi:10.1371/journal.pone.0079736

808 73. Yofe I, Weill U, Meurer M, Chuartzman S, Zalckvar E, Goldman O, et al. One library to
809 make them all: Streamlining the creation of yeast libraries via a SWAp-Tag strategy.
810 Nat Methods. 2016;13: 371–378. doi:10.1038/nmeth.3795

811 74. Sikorski RS, Hieter P. A system of shuttle vectors and yeast host strains designed for
812 efficient manipulation of DNA in Saccharomyces cerevisiae. Genetics. 1989;122: 19–
813 27. doi:10.1080/00362178385380431

814

815 Supplementary material

816 **S1 Fig: (a)** The genetic interaction score (epsilon score) of *SER2* is plotted against the
817 negative LOG_{10} of the *p*-value of the interactions. The volcano plot shows significant negative
818 genetic interactions on the left side of the plot. Dots are color coded according to the respective
819 signaling pathways (orange – TORC1; read – SEA complex, purple – EGO complex, green –
820 unknown signaling pathway). Data are taken from [25].

821 **S2 Source Data Fig 3a:** Data set for serine uptake assays presented in figure 3a

822 **S3 Source Data Fig 3c:** List of all peptides identified including SILAC ratios and intensities.

823 **S4 Source Data Fig 3d:** List of all proteins identified including SILAC ratios and intensities
824 from the comparison of WT and *gnp1Δ* cells.

825 **S5 Fig: (a)** Predicted serine hydroxymethyltransferases (Shm) net fluxes. Variability of net flux
826 through Shm1 and Shm2 at varying serine uptake rates, as predicted by FVA. Positive and
827 negative fluxes correspond to net production of serine and glycine, respectively. Fluxes and
828 serine uptake rates are represented in mmol per gram dry weight per hour.

829 **S6 Source Data Fig 4c:** Data set of serine and glycine levels of WT and *gnp1Δ* cells with and
830 without serine presented in figure 4c.

831

S7 Fig: (a) Tetrad analysis of *ser2Δ* (blue) mutants crossed with Gnp1-mcherry (red). **(b)** Tetrad analysis of *ser2Δ* (blue) mutants crossed with GFP-Gnp1. **(c)** Tetrad analysis of *ser2Δ* (blue) mutants crossed with *gnp1Δ* (red) pRS405-Gnp1 (purple). **(d)** Outline of the position of GFP in the Gnp1 gene. **(e)** Tetrad analysis of *ser2Δ* (blue) mutants crossed with *gnp1Δ* (red) pRS405-*GNP1*$_{211}$*GFP* (green) **(f)** Proteome comparison of lysine labelled WT cells with serine and [$^{13}C_6{}^{15}N_2$]-lysine labelled WT cells depleted of serine. Protein intensities are plotted against normalized SILAC ratios of heavy (-serine) to light (+serine). Significant outliers are colored in red ($p < 1e^{-11}$), orange ($p<1e^{-4}$) or dark blue ($p < 0.05$); other proteins are shown in light blue.

S8 Fig: (a) Tetrad analysis of *gnp1Δ* (red) mutants crossed with *sur2Δ* (orange). **(b)** Tetrad analysis of *ser2Δ* (blue) mutants crossed with *sur2Δ* (orange). **(c)** Tetrad analysis of *gnp1Δ* (red) mutants crossed with *scs7Δ* (orange). **d)** Tetrad analysis of *ser2Δ* (blue) mutants crossed with *scs7Δ* (orange). **(e)** Tetrad analysis of *gnp1Δ* (red) mutants crossed with *sur4*Δ (orange). **(f)** Tetrad analysis of *ser2Δ* (blue) mutants crossed with *sur4Δ* (orange). **(g)** Tetrad analysis of *gnp1Δ* (red) mutants crossed with *lcb4Δ* (orange). **(h)** Tetrad analysis of *ser2Δ* (blue) mutants crossed with *lcb4Δ* (orange). **(i)** Tetrad analysis of *gnp1Δ* (red) mutants crossed with *lcb3Δ* (orange). **(j)** Tetrad analysis of *ser2Δ* (blue) mutants crossed with *lcb3Δ* (orange).

S9 Fig: (a) Serial dilutions of WT, *gnp1Δ* cells, *agp1Δ* cells, *gnp1Δ agp1Δ* cells and two different clones of *pdr5Δ* cells on YPD plates. Control plates (left) and plates containing 1.8 µM cerulenin (right) were used. **(b)** Serial dilutions of WT, *gnp1Δ* cells, *agp1Δ* cells, *gnp1Δ agp1Δ* cells and *fat1Δ* cells on YPD plates. Control plates (left) and plates containing 0.075 µM Aureobasidin A (right) were used.

S10 Source Data Fig 6b: Data set of long chain base levels of WT and *gnp1Δ* cells with and without myriocin presented in figure 6b.

S11 Source Data Fig 6d and e: Data set of serine (6d) and inositol (6e) labelled IPCs presented in figure 6b.

858 **S12 Source Data S4:** List of all proteins identified including SILAC ratios and intensities from
859 the comparison of control cells and serine depleted cells as presented in.

860 **S13 Fig: (a)** Integration of [$^{13}C_3{}^{15}N_1$]-serine into ceramides. Cells were labelled with [$^{13}C_3{}^{15}N_1$]-
861 serine and [$^{2}H_6$]-inositol over 90 minutes in YPD media. Lipids were extracted and analyzed
862 via mass spectrometry. Displayed are the amounts of [$^{13}C_3{}^{15}N_1$]-serine labelled ceramides of
863 WT cells, *gnp1Δ* cells, *gnp1Δagp1Δ* cells and *ser2Δ* cells in mol% per all detected lipids. The
864 average is displayed in bars. Dots correspond to the values of two independent experiments.

865 **S14 Skript:** MATLAB script used for the flux variability analysis.

866

867 **Table 1: List of all yeast strains and their genotypes used in this study.**

	Mat a *his3Δ1 leu2Δ0 met15Δ0 ura3Δ0*	EUROSCARF
	Mat a *his3Δ1 leu2Δ0 met15Δ0 ura3Δ0 ser1Δ::KAN*	EUROSCARF
	Mat a *his3Δ1 leu2Δ0 met15Δ0 ura3Δ0 ser2Δ::KAN*	EUROSCARF
	Mat a *his3Δ1 leu2Δ0 met15Δ0 ura3Δ0 ser3Δ::KAN*	EUROSCARF
	Mat a *his3Δ1 leu2Δ0 met15Δ0 ura3Δ0 ser33Δ::KAN*	EUROSCARF
TWY138	Mat a *ura3-52 trp1Δ 2 leu2-3112 his3-11 ade2-1 can1-100*	Walther et al. 2007
TWY139	Mat α *ura3-52 trp1Δ 2 leu2-3112 his3-11 ade2-1 can1-100*	Walther et al. 2007
FFY1260	Mat a/α *ura3-52/ura3-52; trp1Δ 2/trp1Δ 2; leu2-3,112/leu2-3,112; his3-11/his3-11; ade2-1/ade2-1; can1-100/can1-100 SER2/ser2Δ::KAN GNP1/gnp1Δ::NAT*	this study
FFY1420	Mat a/α *ura3-52/ura3-52; trp1Δ 2/trp1Δ 2; leu2-3,112/leu2-3,112; his3-11/his3-11; ade2-1/ade2-1; can1-100/can1-100 AGP1/agp1Δ::HPH GNP1/gnp1Δ::NAT SER2/ser2Δ::KAN*	this study
FFY1534	Mat a/α *ura3-52/ura3-52; trp1Δ 2/trp1Δ 2; leu2-3,112/leu2-3,112; his3-11/his3-11; ade2-1/ade2-1; can1-100/can1-100 AGP1/agp1Δ::HPH SER2/ser2Δ::KAN*	this study
FFY2104	Mat a/α *ura3-52/ura3-52; trp1Δ 2/trp1Δ 2; leu2-3,112/leu2-3,112; his3-11/his3-11; ade2-1/ade2-1; can1-100/can1-100 ORM1/orm1 Δ::NAT ORM2/orm2 Δ::HPH AGP1/agp1Δ::HIS GNP1/gnp1Δ::KAN*	this study
FFY2306	Mat a/α *ura3-52/ura3-52; trp1Δ 2/trp1Δ 2; leu2-3,112/leu2-3,112; his3-11/his3-11; ade2-1/ade2-1; can1-100/can1-100 SER2/ser2Δ::KAN GNP1/Gnp1-mcherry::KAN*	this study

FFY1901	Mat a/α *ura3-52/ura3-52; trp1Δ 2/trp1Δ 2; leu2-3,112/leu2-3,112; his3-11/his3-11; ade2-1/ade2-1; can1-100/can1-100 SER2/ser2Δ::NAT SUR2/sur2Δ::KAN*	this study
FFY1902	Mat a/α *ura3-52/ura3-52; trp1Δ 2/trp1Δ 2; leu2-3,112/leu2-3,112; his3-11/his3-11; ade2-1/ade2-1; can1-100/can1-100 GNP1/gnp1Δ::NAT SUR2/sur2Δ::KAN*	this study
FFY1897	Mat a/α *ura3-52/ura3-52; trp1Δ 2/trp1Δ 2; leu2-3,112/leu2-3,112; his3-11/his3-11; ade2-1/ade2-1; can1-100/can1-100 SER2/ser2Δ::NAT SCS7/scs7Δ::KAN*	this study
FFY1898	Mat a/α *ura3-52/ura3-52; trp1Δ 2/trp1Δ 2; leu2-3,112/leu2-3,112; his3-11/his3-11; ade2-1/ade2-1; can1-100/can1-100 GNP1/gnp1Δ::NAT SCS7/scs7Δ::KAN*	this study
FFY1899	Mat a/α *ura3-52/ura3-52; trp1Δ 2/trp1Δ 2; leu2-3,112/leu2-3,112; his3-11/his3-11; ade2-1/ade2-1; can1-100/can1-100 SER2/ser2Δ::NAT SUR4/sur4Δ::KAN*	this study
FFY1900	Mat a/α *ura3-52/ura3-52; trp1Δ 2/trp1Δ 2; leu2-3,112/leu2-3,112; his3-11/his3-11; ade2-1/ade2-1; can1-100/can1-100 GNP1/gnp1Δ::NAT SUR4/sur4Δ::KAN*	this study
FFY2051	Mat a/α *ura3-52/ura3-52; trp1Δ 2/trp1Δ 2; leu2-3,112/leu2-3,112; his3-11/his3-11; ade2-1/ade2-1; can1-100/can1-100 SER2/ser2Δ::KAN LCB4/lcb4Δ::NAT*	this study
FFY2152	Mat a/α *ura3-52/ura3-52; trp1Δ 2/trp1Δ 2; leu2-3,112/leu2-3,112; his3-11/his3-11; ade2-1/ade2-1; can1-100/can1-100 GNP1/gnp1Δ::KAN LCB4/lcb4Δ::NAT*	this study
FFY2144	Mat a/α *ura3-52/ura3-52; trp1Δ 2/trp1Δ 2; leu2-3,112/leu2-3,112; his3-11/his3-11; ade2-1/ade2-1; can1-100/can1-100 SER2/ser2Δ::NAT LCB3/lcb3Δ::KAN*	this study
FFY2146	Mat a/α *ura3-52/ura3-52; trp1Δ 2/trp1Δ 2; leu2-3,112/leu2-3,112; his3-11/his3-11; ade2-1/ade2-1; can1-100/can1-100 GNP1/gnp1Δ::NAT LCB3/lcb3Δ::KAN*	this study
FFY2501	Mat a/α *ura3-52/ura3-52; trp1Δ 2/trp1Δ 2; leu2-3,112/leu2-3,112; his3-11/his3-11; ade2-1/ade2-1; can1-100/can1-100 SER2/ser2Δ::KAN GNP1/gnp1Δ::NAT* pRS405-GNP1	this study
FFY2489	Mat a/α *ura3-52/ura3-52; trp1Δ 2/trp1Δ 2; leu2-3,112/leu2-3,112; his3-11/his3-11; ade2-1/ade2-1; can1-100/can1-100 SER2/ser2Δ::KAN GNP1/gnp1Δ::NAT* pRS405-GNP1$_{211}$GFP	this study
FFY2577	*his3Δ 1/his3Δ 1 leu2Δ 0/ leu2Δ 0 lys2Δ 0/ lys2Δ 0 ura3Δ/ura3Δ GFP-Gnp1 SER2/ser2Δ::NAT*	this study
	MATα his3Δ1 leu2Δ0 lys2Δ0 ura3Δ0 GFP-GNP1	[73]
FFY1254	Mat α *ura3-52 trp1Δ 2 leu2-3112 his3-11 ade2-1 can1-100 ser2Δ::KAN*	this study
FFY1251	Mat a *ura3-52 trp1Δ 2 leu2-3112 his3-11 ade2-1 can1-100 gnp1Δ::NAT*	this study
FFY1545	Mat a *ura3-52 trp1Δ 2 leu2-3112 his3-11 ade2-1 can1-100 agp1Δ::HPH gnp1Δ::NAT*	this study

FFY1533	Mat a *ura3-52 trp1Δ 2 leu2-3112 his3-11 ade2-1 can1-100 agp1Δ::HPH*	this study
FFY1861	Mat a *ura3-52 trp1Δ 2 leu2-3112 his3-11 ade2-1 can1-100 orm1Δ::NAT orm2Δ::HPH*	this study
FFY1815	Mat α *ura3-52 trp1Δ 2 leu2-3112 his3-11 ade2-1 can1-100 gnp1Δ::KAN*	this study
FFY1058	Mat α *ura3-52 trp1Δ 2 leu2-3112 his3-11 ade2-1 can1-100 fat1Δ::NAT*	this study
FFY1422	Mat α *ura3-52 trp1Δ 2 leu2-3112 his3-11 ade2-1 can1-100* Gnp1-mcherry::KAN	this study
FFY978	Mat α *ura3-52 trp1Δ 2 leu2-3112 his3-11 ade2-1 can1-100 sur2Δ::NAT*	this study
FFY1829	Mat α *ura3-52 trp1Δ 2 leu2-3112 his3-11 ade2-1 can1-100 scs7Δ::NAT*	this study
FFY197	Mat α *ura3-52 trp1Δ 2 leu2-3112 his3-11 ade2-1 can1-100 sur4Δ::NAT*	this study
FFY1978	Mat α *ura3-52 trp1Δ 2 leu2-3112 his3-11 ade2-1 can1-100 lcb4Δ::KAN*	this study
FFY2102	Mat α *ura3-52 trp1Δ 2 leu2-3112 his3-11 ade2-1 can1-100 lcb3Δ::NAT*	this study
FFY1816	Mat α *ura3-52 trp1Δ 2 leu2-3112 his3-11 ade2-1 can1-100 ser2Δ::NAT*	this study
FFY2439	*ura3Δ0; leu2Δ0; his3Δ1; met15Δ0 ser2Δ::NAT*	this study
SEY6210	Mat α *leu2-3,112 ura3-52 his3-Δ200 trp-Δ901 lys2-801 suc2-Δ9 GAL*	Robinson et al. 1988
FFY727	Mat α *leu2-3,112 ura3-52 his3-Δ200 trp1-Δ901 suc2-Δ9 lys2-801; GAL gnp1Δ::NAT*	this study
FFY848	Mat α *leu2-3,112 ura3-52 his3-Δ200 trp-Δ901 lys2-801 suc2-Δ9 GAL ser2Δ::KAN*	this study
FFY1379	Mat α *leu2-3,112 ura3-52 his3-Δ200 trp-Δ901 lys2-801 suc2-Δ9 GAL ser2Δ::KAN*	this study
FFY1375	Mat α *leu2-3,112 ura3-52 his3-Δ200 trp-Δ901 lys2-801 suc2-Δ9 GAL agp1Δ::KAN*	this study
FFY1385	Mat α *leu2-3,112 ura3-52 his3-Δ200 trp-Δ901 lys2-801 suc2-Δ9 GAL gnp1Δ::NAT agp1Δ::HPH*	this study
FFY2337	Mat α *leu2-3,112 ura3-52 his3-Δ200 trp-Δ901 lys2-801 suc2-Δ9 GAL pdr5Δ::NAT*	this study
FFY2338	Mat α *leu2-3,112 ura3-52 his3-Δ200 trp-Δ901 lys2-801 suc2-Δ9 GAL pdr5Δ::HPH*	this study
FFY2150	Mat α *leu2-3,112 ura3-52 his3-Δ200 trp-Δ901 lys2-801 suc2-Δ9 GAL* pHLUK pRS414	this study
FFY2151	Mat α *leu2-3,112 ura3-52 his3-Δ200 trp1-Δ901 suc2-Δ9 lys2-801; GAL gnp1Δ::NAT* pHLUK pRS414	this study
FFY2152	Mat α *leu2-3,112 ura3-52 his3-Δ200 trp-Δ901 lys2-801 suc2-Δ9 GAL agp1Δ::KAN* pHLUK pRS414	this study
FFY2153	Mat α *leu2-3,112 ura3-52 his3-Δ200 trp-Δ901 lys2-801 suc2-Δ9 GAL gnp1Δ::NAT agp1Δ::HPH* pHLUK pRS414	this study

868

869 **Table 2: List of all plasmids used in this study.**

	pHLUK	ADDGENE
	pRS414	[74]
	pRS405	[74]
FFP255	pRS405-GNP1	this study
FFP286	pRS405-GNP1$_{211}$GFP	this study

870

871

872 # Fig captions

873 **Fig 1: Serine metabolism is essential for sphingolipid homeostasis in yeast. (a)** Model of
874 serine metabolism via the 3-phospho-glycerate pathway. **(b)** Serial dilutions of knockouts of
875 serine biosynthesis genes in the presence (control) or absence of serine (- serine) on synthetic
876 medium. The strains used are from top to bottom: wild-type (WT;SEY6210), *ser1Δ*, *ser2Δ*,
877 *ser3Δ* and *ser33Δ*. **(c)** Model of sphingolipid (SP) metabolism in yeast. Myriocin (red) is an
878 inhibitor of the SPT (Lcb1, Lcb2, Tsc3). **(d)** Exogenous serine is essential for survival under
879 SP depleted conditions. Serial dilutions of WT and *ser2Δ* cells on synthetic medium. Control
880 plates (upper left), plates without serine (upper right panel), plates containing 1 µM myriocin
881 (lower right) and plates containing 1 µM myriocin with no serine available (lower right) are
882 displayed.

883 **Fig 2: GNP1 genetically interacts with serine metabolism. (a)** Outline for the identification
884 of the plasma membrane serine transporter in yeast. WT cells (I, upper left) as well as *SER2*
885 knockout cells (II, upper right) and knockouts of the serine transporter in yeast (gene XXX, III
886 lower left) should grow fine. Deletion of both, *SER2* and the serine transporter should result in
887 synthetic lethality (IV, lower right). **(b)** The genetic interaction score (epsilon score) of *SER2* is
888 plotted against the negative LOG_{10} of the P-value of the interactions. The volcano plot shows
889 significant negative genetic interactions on the left side of the plot. Highly significant

interactions are shown in green. Data are taken from (25). **(c)** Tetrad analysis of *gnp1Δ* (red) mutants crossed with *ser2Δ* (blue). **(d)** Tetrad analysis of *agp1Δ* (green) mutants crossed with *ser2Δ* (blue). **(e)** Tetrad analysis of *ser2Δ* (blue) mutants crossed with *gnp1Δagp1Δ* (red and green, respectively).

Fig 3: Gnp1 and Agp1 are essential for the uptake of exogenous serine. (a) WT cells (black line), *gnp1Δ* cells (red line), *agp1Δ* cells (green line) and *gnp1Δagp1Δ* cells (purple line) were grown in synthetic complete medium. Cells were washed and incubated with [^{14}C]-serine. The uptake rate of [^{14}C]-serine was measured. Error bars correspond to standard deviations. n=3. **(b)** Schematic outline of the main serine consuming and producing processes. **(c)** WT cells (black line), *gnp1Δ* cells (red line) and *ser2Δ* cells (blue line) were grown in the presence of stable isotope labelled, [$^{13}C_3{}^{15}N_1$]-serine. Graphs represent the density function of the rates of [$^{13}C_3{}^{15}N_1$]-serine incorporation into all peptides containing a single serine. **(d)** Proteome comparison of lysine labeled WT cells and [$^{13}C_6{}^{15}N_2$]-lysine labeled *gnp1Δ* cells. Protein intensities are plotted against normalized SILAC ratios of heavy (*gnp1Δ*) to light (WT). Significant outliers are colored in red ($p < 1e^{-11}$), orange ($p<1e^{-4}$) or dark blue ($p < 0.05$); other proteins are shown in light blue.

Fig 4: Intracellular serine concentrations are dependent on serine uptake (a) Predicted fluxes of serine. Flux variability of metabolic reactions, which produce or consume serine, as predicted by flux variability analysis (FVA). Positive and negative fluxes correspond to serine production and consumption, respectively. Fluxes are represented in mmol per gram dry weight per hour. **(b)** Predicted net flux of serine producing reactions at varying serine uptake rates. Variability of net flux through Shm1, Shm2 and Ser2 at varying serine uptake rates, as predicted by FVA. Positive and negative fluxes correspond to serine production and consumption, respectively. Fluxes and serine uptake rates are represented in mmol per gram dry weight per hour. **(c)** Cellular serine and glycine concentrations. Prototroph WT and *gnp1Δ* cells were grown in the absence of amino acids and with and without serine. Serine and glycine concentrations from whole cell lysates were analyzed by mass spectrometry. Error bars

represent standard deviations. n=3. *, P-value <0.05, calculated from t-test. Differences between data that are not labelled with a star are not significant.

Fig 5: Gnp1 dependent serine uptake is essential to maintain sphingolipid homeostasis. **(a)** Serial dilutions of WT, *gnp1Δ* cells, *agp1Δ* cells and *gnp1Δagp1Δ* cells on synthetic medium. Control plates (upper left), plates without serine (upper right), plates containing 1 µM myriocin (lower left) and plates containing 1 µM myriocin with no serine available (lower right) are displayed. **(b)** Serial dilutions of WT, *gnp1Δ* cells, *agp1Δ* cells and *gnp1Δagp1Δ* cells on YPD medium. Control plates (left), plates containing 0.5 µM myriocin (middle) and plates containing 0.5 µM myriocin and 25 µM phytosphingosine (PHS) (right) are displayed. **(c)** Serial dilutions of prototroph WT, *gnp1Δ* cells, *agp1Δ* cells and *gnp1Δagp1Δ* cells on plates without amino acids (upper row) and plates without amino acids (-AAs) with serine (lower row), each with 0.5 µM (middle) and 1.5 µM myriocin (right). **(d)** Tetrad analysis of *orm1Δorm2Δ* cells (dark blue and yellow, respectively crossed with *gnp1Δ* (red) cells and followed by the deletion of *AGP1* (green).

Fig 6: Imported serine is the main source for SP biosynthesis (a). Predicted flux of SPT at varying serine uptake rates. Variability of flux through SPT at varying serine uptake rates, as predicted by FVA. Positive and negative fluxes correspond to serine production and consumption, respectively. SPT fluxes and serine uptake rates are represented in mmol per gram dry weight per hour. **(b)** GNP1 is essential to maintain SP homeostasis. Mass spectrometric analysis of phytosphingosine (PHS) concentrations in WT and *gnp1Δ* cells grown in the presence or absence of 0.25 µM myriocin or 0.025 µM myriocin in YPD medium. Error bars represent standard deviations. n=3. *, P-value <0.05, calculated from t-test. **(c)** Model of SPT activity under high and low concentrations of myriocin. Under high concentrations of myriocin (left panel) most SPT complexes are inhibited by myriocin and de novo SP biosynthesis is significantly impaired resulting in decreased SP concentrations. Under low concentrations of myriocin (right panel), only few SPT complexes are inhibited by the suicide inhibitor myriocin while the cell regulates against the decreasing SP levels resulting in

944 the upregulation of the remaining SPT molecules and constant SP concentrations. **(d)**
945 Integration of [$^{13}C_3{}^{15}N_1$]-serine into inositol-phosphorylceramides (IPC). Cells were labelled
946 with [$^{13}C_3{}^{15}N_1$]-serine and [$^{2}H_6$]-inositol over 90 minutes in YPD medium. Lipids were extracted
947 and analyzed via mass spectrometry. Displayed are the amounts of [$^{13}C_3{}^{15}N_1$]-serine labelled
948 IPCs of WT cells, *gnp1Δ* cells, *gnp1Δagp1Δ* cells and *ser2Δ* cells in mol% per all detected
949 lipids. The average is displayed in bars. Dots correspond to the values of two independent
950 experiments. (e) Integration of [$^{2}H_6$]-inositol into IPCs. Displayed are the amounts of [2H6]-
951 inositol labelled IPCs of WT cells, *gnp1Δ* cells, *gnp1Δagp1Δ* cells and *ser2Δ* cells in mol% per
952 all detected lipids. The average is displayed in bars. Dots correspond to the values of two
953 independent experiments.

954 **Fig 7: Model for direct coupling of Gnp1 mediated serine uptake and regulated SP**
955 **biosynthesis.** SP biosynthesis is directly coupled to Gnp1-mediated serine uptake. The SPT
956 pool at the cortical ER is highly regulated by serine uptake and the TORC1/Ypk1/Orm1/2
957 signaling network. The nuclear envelope localized SPT pool is responsible for constant SP
958 biosynthesis. This model adds serine uptake as another factor to previously described
959 mechanisms regulating SP homeostasis by the signaling cascade of Slm1/2-TORC2-Ypk1/2
960 and the Orm proteins (7–9).

961

a

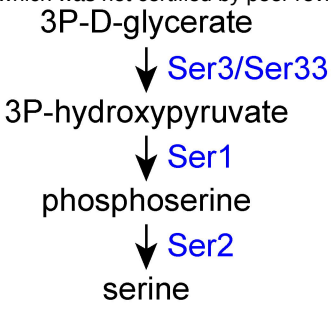

b

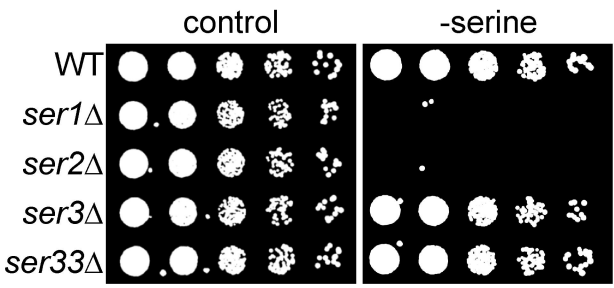

c

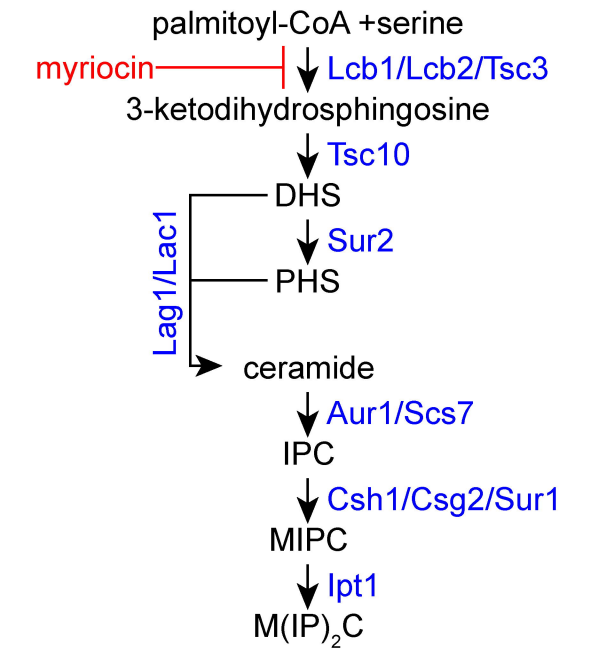

d

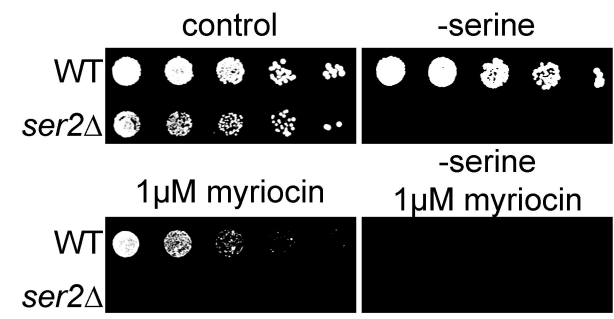

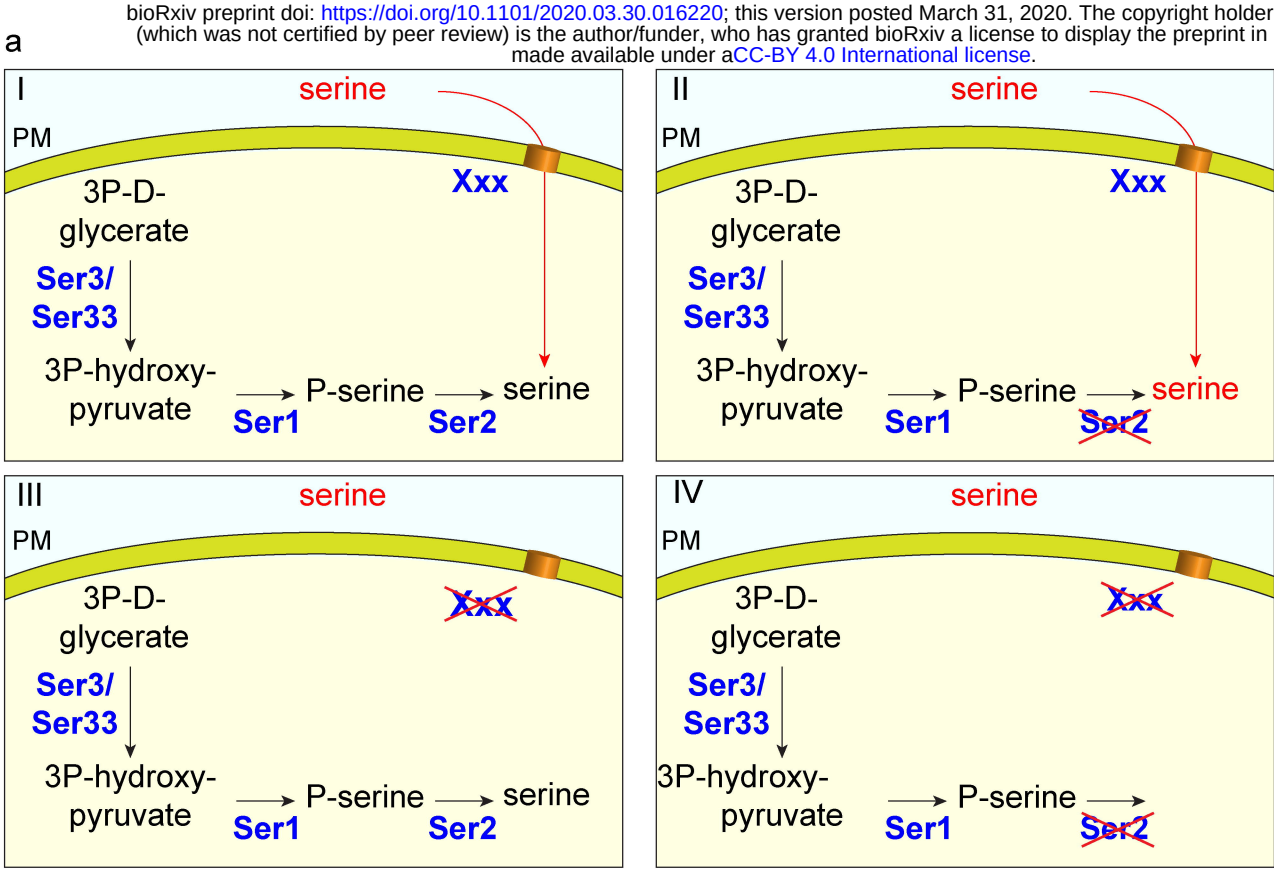

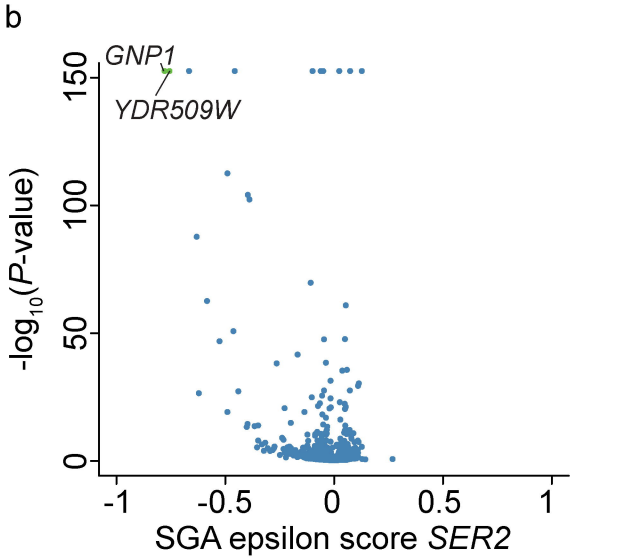

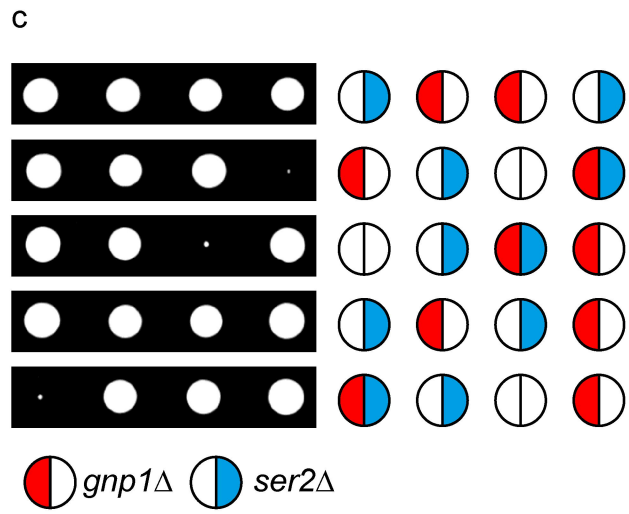

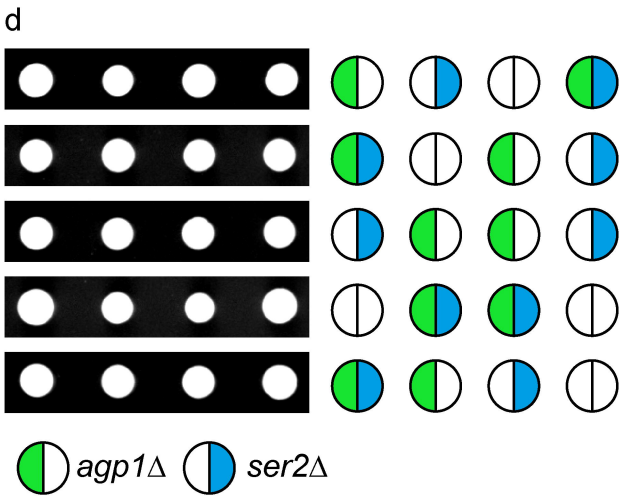

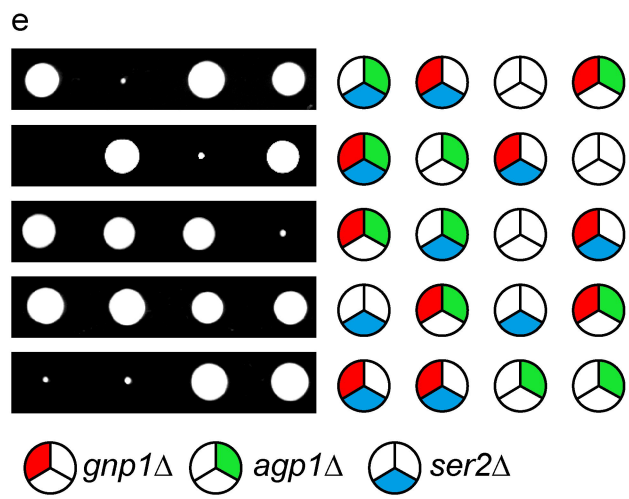

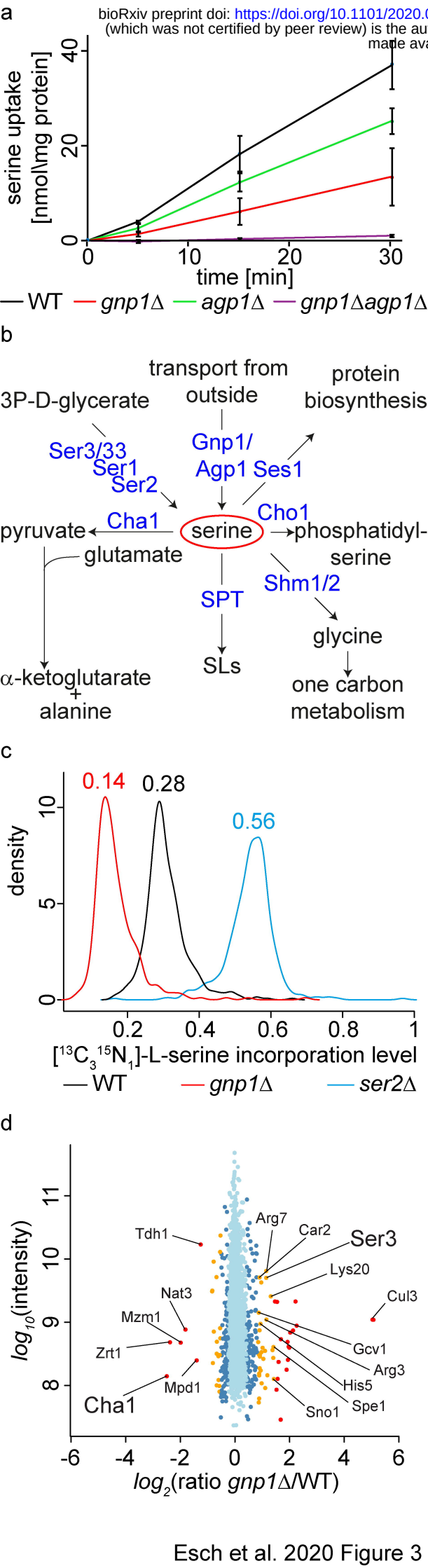

Esch et al. 2020 Figure 3

a

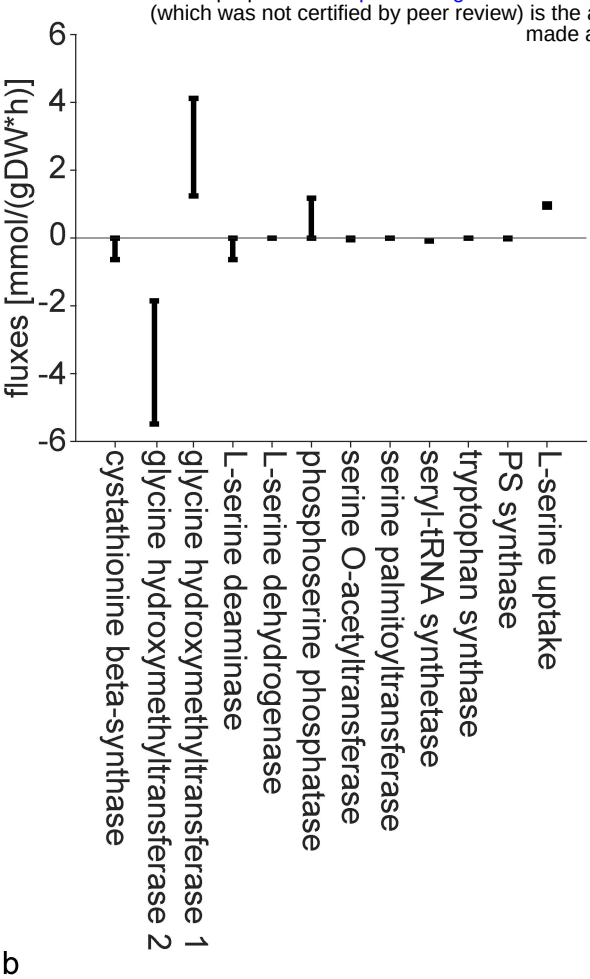

b

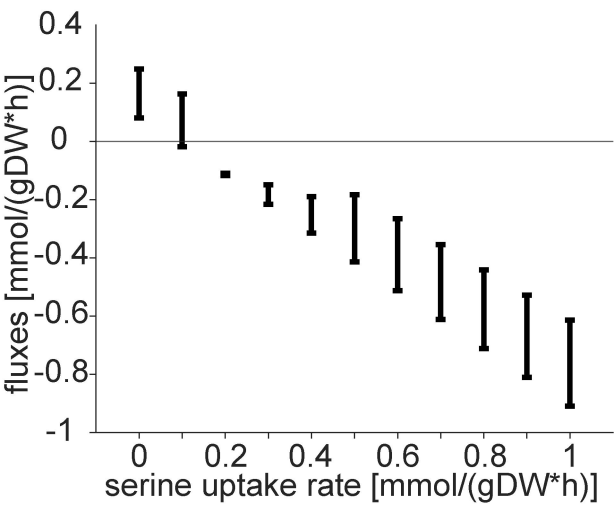

c

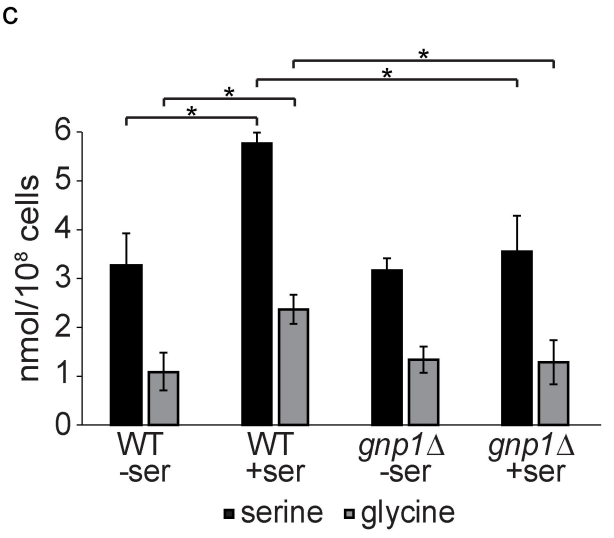

a

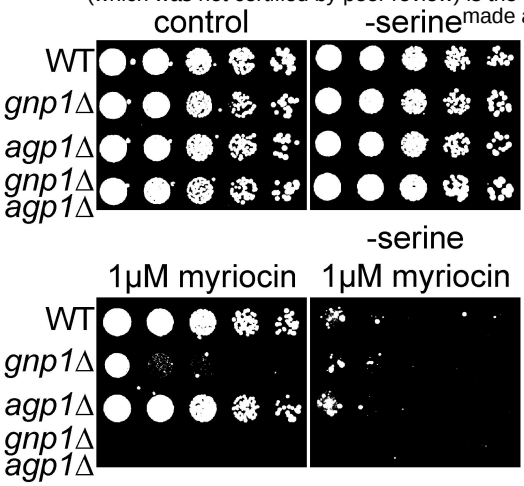

b

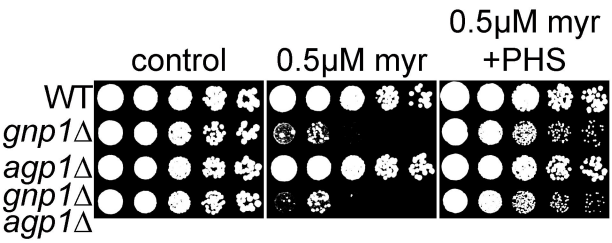

c

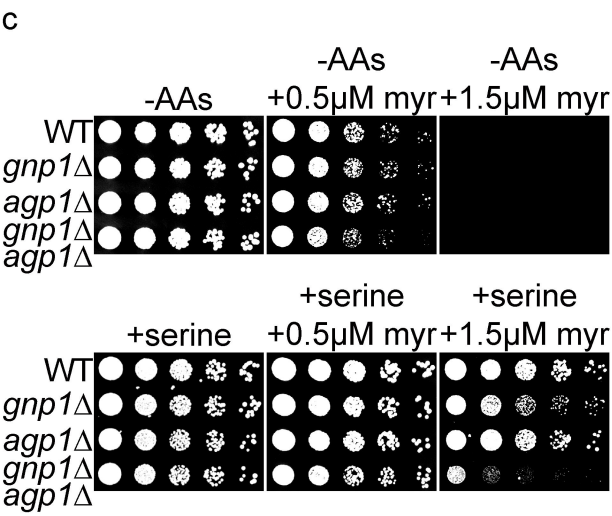

d

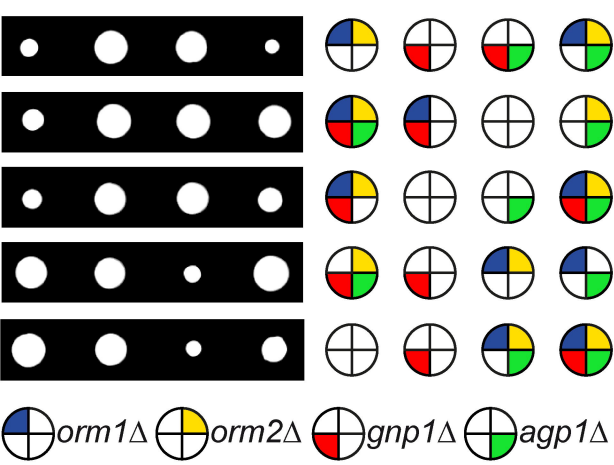

a

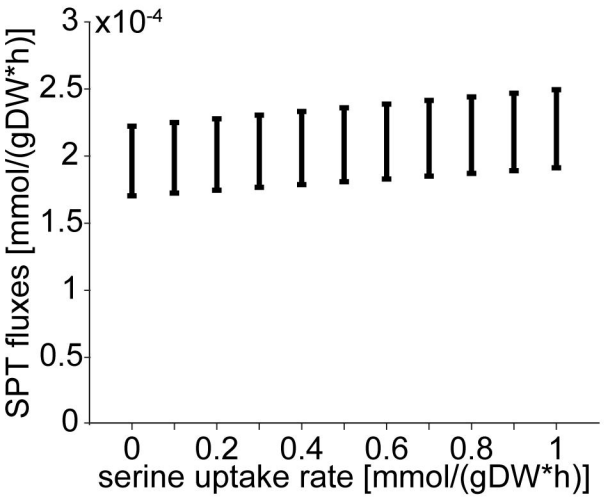

b

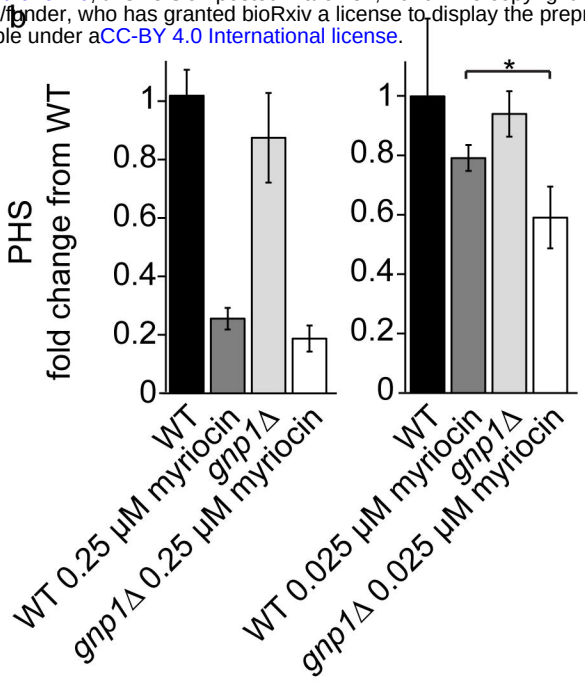

c

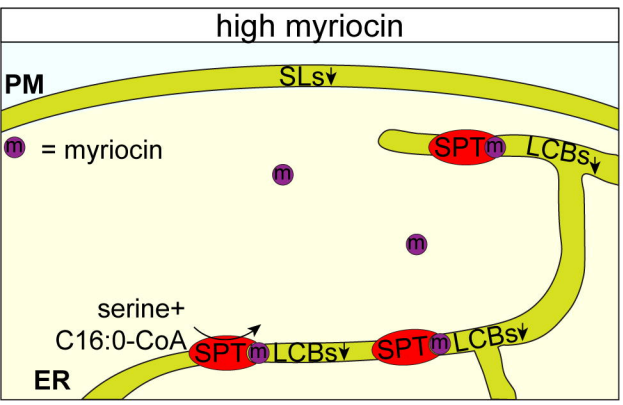

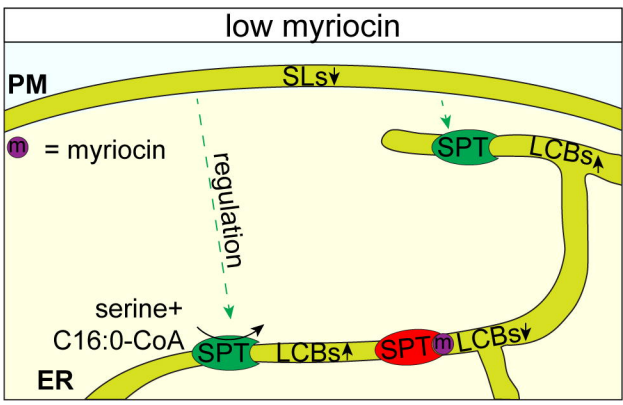

d

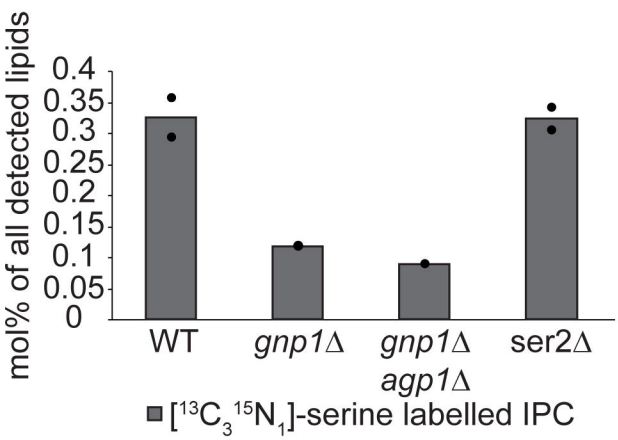

e

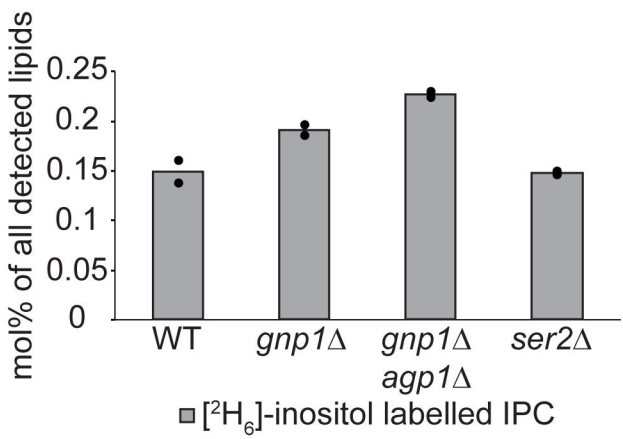

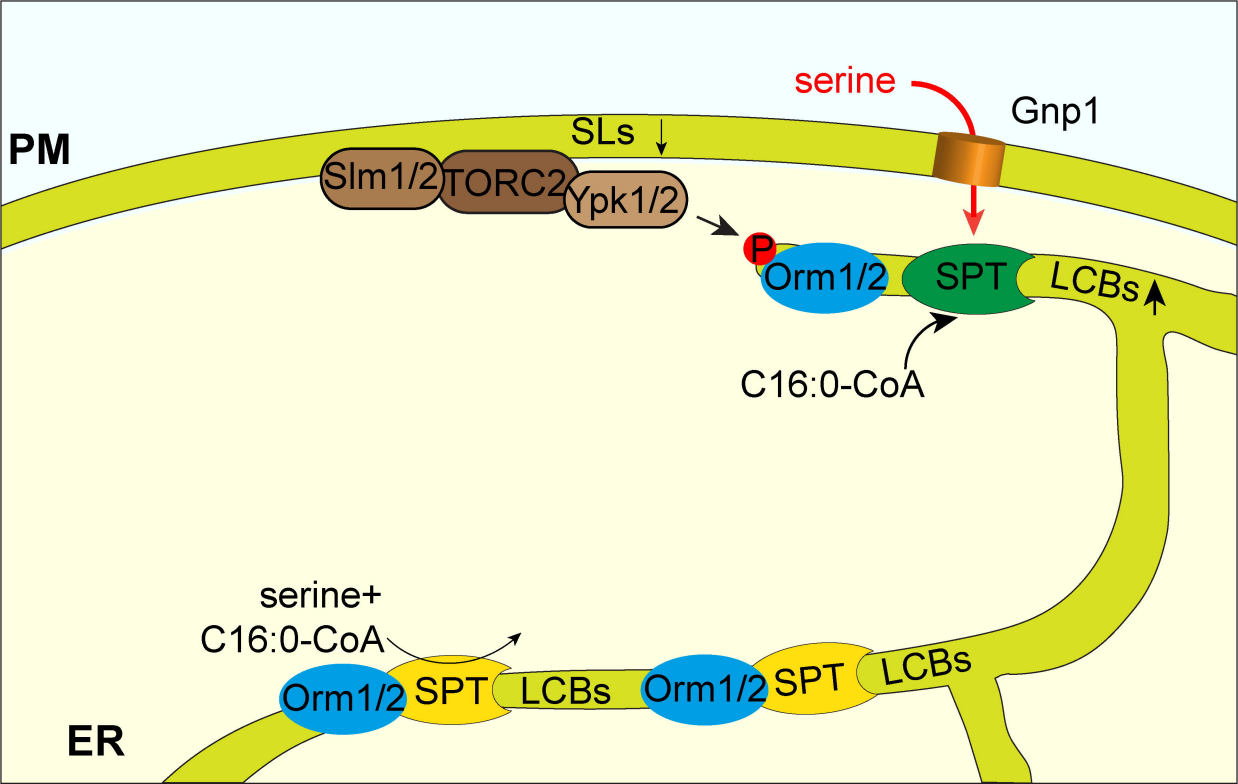
PM
SLs
Slm1/2
TORC2
Ypk1/2
serine
Gnp1
P
Orm1/2
SPT
LCBs
C16:0-CoA
serine+
C16:0-CoA
Orm1/2
SPT
LCBs
Orm1/2
SPT
LCBs
ER